

BL7U

## ARPES Studies of Quasi-Particle Dynamics in Topological Insulators

S. R. Park<sup>1</sup>, W. S. Jung<sup>1</sup>, G. R. Han<sup>1</sup>, Y. K. Kim<sup>1</sup>, Ch. Kim<sup>1</sup>, D. J. Song<sup>1</sup>, Y. Y. Koh<sup>1</sup>, C. Kim<sup>1</sup>, S. Kimura<sup>2</sup>, K. D. Lee<sup>3</sup>, N. Hur<sup>3</sup>, J. Y. Kim<sup>4</sup>, B. K. Cho<sup>4</sup>, J. H. Kim<sup>5</sup>, Y. S. Kwon<sup>5</sup>, J. H. Han<sup>5</sup>

<sup>1</sup>*Institute of Physics and Applied Physics, Yonsei University, Seoul, Korea*

<sup>2</sup>*UVSOR Facility, Institute for Molecular Science, Okazaki 444-8585, Japan*

<sup>3</sup>*Department of Physics, Inha University, Incheon, Korea*

<sup>4</sup>*Department of Materials Science & Engineering, GIST, Gwangju, Korea*

<sup>5</sup>*Department of Physics, Sungkyunkwan University, Suwon, Korea*

Topological insulators (TIs) are a new class of materials which always have metallic surface states. These metallic surface states are protected by the time reversal symmetry and have their spins locked into the momentum. The latter fact brings about suppression of back scattering and quasi-particles are expected to have a longer life time. An experimental verification of this fact is essential to understand the novel properties of the metallic states, and therefore we have performed temperature and photon energy dependent angle resolved photoemission (ARPES) experiments on various TIs.

$\text{Bi}_2\text{Se}_3$ ,  $\text{Bi}_2\text{Te}_3$  and Sb single crystals were grown by flux and Bridgman methods. Samples were cleaved in situ and ARPES measurements were performed at the beam line 7U [1][2]. Samples were sometimes left in the vacuum for a few days to age the surface.

Figure 1(a) shows ARPES data from a freshly cleaved surface of  $\text{Bi}_2\text{Se}_3$  taken with 8 eV photons. At 8 eV, the photoemission matrix element for the bulk states is suppressed that the bulk signal is very weak (intensity at the  $\Gamma$  point near the Fermi energy). The cone shape and fast dispersing band is the surface metallic states. The surface band reaches the  $\Gamma$  point near the 0.3 eV binding energy. This point is called the Dirac point. After exposing the surface to a relatively poor vacuum for 4 days ages the surface, ARPES data was retaken and is shown in figure 1(b). Note that the Dirac point has shifted to a higher binding energy side by about 0.1 eV. This is due to the electron doping effect by the adsorbed atoms and molecules on the surface.

Suppression of the bulk ARPES states allows us to perform reliable self energy analysis on the data. The imaginary parts of the self energies from the data are plotted in figure 2(a). In the data, it is noted that  $\text{Im}\Sigma$  initially increases but then decreases near the bulk band bottom energy (dashed lines). This is true for both fresh and aged surfaces and thus strongly indicates that the kinks are related to the bulk states. The scattering of the quasi-particles in the metallic surface states can be analyzed in terms of electron-electron, electron-phonon and impurity scatterings. The analysis results in figure 2(b) show that the quasi-particles in the surface states mostly decay to the bulk states but not to other surface states.

Even though the above results provide us valuable information, we still do not have the intrinsic properties because the quasi-particle dynamics is dominated by the coupling to the bulk states. To overcome this, we performed ARPES on higher quality TIs, e.g.,  $\text{Bi}_2\text{Te}_3$  shown in figure 1(a). The result plotted in figure 2(a) along with the result from Sb show that the scattering rate is more or less binding energy independent. This constant term is attributed to the contribution from uneven surfaces, thus an extrinsic effect. These results strongly suggest that the intrinsic life time of the quasi-particles in surface states is extremely long. This is an important property for TIs as the candidate materials for the future spintronic applications.

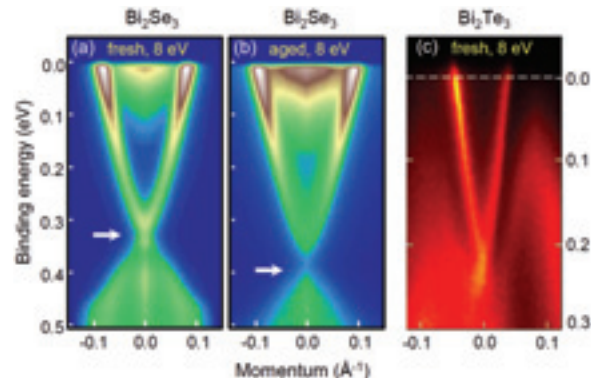


Fig. 1. ARPES data near the  $\Gamma$  point from TIs under various conditions.  $\text{Bi}_2\text{Se}_3$  data from (a) fresh and (b) aged surfaces. (c) Data from fresh  $\text{Bi}_2\text{Te}_3$  surface.

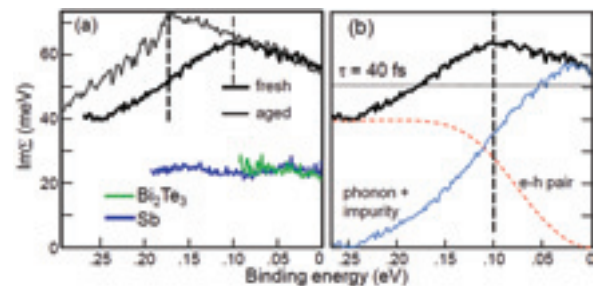


Fig. 2. (a) Imaginary parts of the self energy from various TIs. (b) Contributions from various scattering channels.

[1] S. R. Park *et al.*, Phys. Rev. B **81** (2010) 041405.

[2] S. R. Park *et al.*, in preparation.

## Characterization of Calcium in Huntite by an XAFS Method

T. Kurisaki<sup>1</sup>, D. Tanaka<sup>1</sup>, S. Kokubu<sup>1</sup> and H. Wakita<sup>1,2</sup>

<sup>1</sup>*Department of Chemistry, Faculty of Science, Fukuoka University, Jonan-ku, Fukuoka 814-0180, Japan*

<sup>2</sup>*Advanced Materials Institute, Fukuoka University, Jonan-ku, Fukuoka 814-0180, Japan*

A huntite was called ‘a hanto-ishi’ and was used as a pigment of the white in ancient Egypt. This mineral chemical formula is expressed in  $\text{CaMg}_3(\text{CO}_3)_2$ . The huntite has very few reports about locality, and it is a rare mineral. However, this mineral is used abundantly in ancient Egypt. It is not apparent why the huntite which is a rare mineral was used as a pigment of the white. It is reported that the huntite is produced in Nagasaki. For various light element compounds, we have studied the electronic structure by X-ray absorption spectroscopy [1]. These results suggested that there is a correlation between XANES spectra and the local structures.

In this work, we performed the XANES spectra measurement about various calcium salts and minerals such as huntite and dolomite. The obtained experimental XANES spectra are analyzed using the calculated theoretical spectra from DV-X $\alpha$  calculations. The X-ray absorption spectra were measured at BL1A of the UVSOR in the Institute of Molecular Science, Okazaki [4]. The ring energy of the UVSOR storage ring was 750MeV and the stored current was 110-230 mA. P K-edge absorption spectra were recorded in the regions of 2125-2270eV by use of two InSb crystals. The absorption was monitored by the total electron yield using a photomultiplier. The samples were spread into the carbon tape on the first photodiode made of CuBe of the photomultiplier. Figure 1 shows the observed Ca K-edge XANES spectra for the Huntite and Dolomite. The Ca-K XANES spectra of Huntite and Dolomite show different peak profiles. This result shows that the calcium in these minerals has different electronic states. We are going to try to calculate the spectra by DV-X $\alpha$  molecular orbital calculations. The calculated XANES spectra and the observed XANES spectra of the Huntite and the Dolomite are shown in Fig. 2. The observed XANES spectra and the calculated XANES spectra showed good agreement. The peaks A and B are estimated to the electron transition (mainly Ca 1s to unoccupied mixed orbital consisting of O 3d, O 3p, O 3s and O 4s).

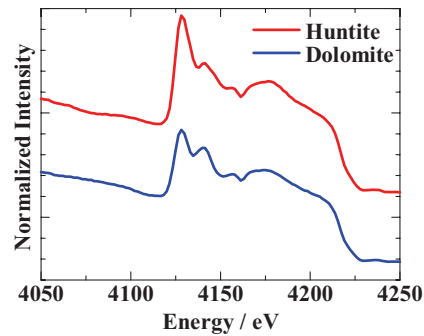


Fig. 1. Observed Ca K-edge XANES spectra of Huntite and Dolomite.

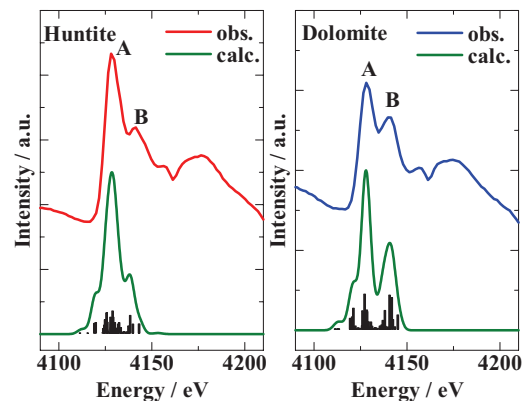


Fig. 2. The comparison of observed XANES spectra with calculated XANES spectra for Ca K-edge.

[1] T. Kurisaki, S. Matsuo, I. Toth and H. Wakita, *Anal. Sci.* **24** (2008) 1385.

[2] S. Murata, T. Matsukawa, S. Naoè, T. Horigome, O. Matsudo and M. Watatabe, *Rev. Sci. Instrum.* **63** (1992) 1309.

## Excitonic Structures of PbMoO<sub>4</sub> and PbWO<sub>4</sub> Crystals

M. Fujita<sup>1</sup>, M. Itoh<sup>2</sup>, H. Mitani<sup>2</sup>, Sangeeta<sup>3</sup> and M. Tyagi<sup>3</sup>

<sup>1</sup>Japan Coast Guard Academy, Kure 737-8512, Japan

<sup>2</sup>Dept. of Electrical and Electronic Engineering, Shinshu University, Nagano 380-8553, Japan

<sup>3</sup>Crystal Technology Laboratory, Bhabha Atomic Research Center, Mumbai 400 085, India

Metal tungstates and molybdates are widely used for scintillation detectors. Therefore information on the exciton states is deeply desired to understand the de-excitation processes after high-energy electronic excitation in these materials. PbWO<sub>4</sub> and PbMoO<sub>4</sub> crystallize in the scheelite structure. We found that PbWO<sub>4</sub> exhibits a pronounced exciton band with distinct dichroism, and proposed that the exciton transition is explained in terms of the cationic Pb 6s → 6p excitation [1]. In the present study, reflectivity spectra of PbMoO<sub>4</sub> crystals are measured in order to get more detailed information on the excitonic structures in Pb compounds.

Figure 1 shows reflectivity spectra of PbMoO<sub>4</sub> up to 20 eV measured with the light polarized parallel to the *a*-axis (**E**//*a*) and *c*-axis (**E**//*c*). Remarkable dichroism is seen in the region below 6 eV. In Fig. 2 are presented the imaginary-part  $\epsilon_2$  spectra of the dielectric function calculated from the spectra in Fig. 1 using a Kramers-Kronig analysis. The lowest exciton band 1 for **E**//*a* has two peaks *a*<sub>1</sub> and *a*<sub>2</sub>. On the other hand, the spectrum for **E**//*c* exhibits a weak plateau in this region. The  $\epsilon_2$  spectra of PbWO<sub>4</sub> [1] are also shown in Fig. 2 for the sake of comparison. Common features are observed between the structures in PbMoO<sub>4</sub> and PbWO<sub>4</sub>; i. e. the lowest band 1 shows doublet structure for **E**//*a* and the band 2 is observed for **E**//*c*.

Theoretical calculation of the electronic structure of PbMoO<sub>4</sub> (PbWO<sub>4</sub>) by the DV-*X* $\alpha$  method indicates that the valence band and the conduction band are mainly composed of O 2p and Mo 4d (W 5d) states, respectively, and the Pb state contributes appreciably to the top of the valence band and the bottom of the conduction band [2]. Similarity of the optical spectra in Fig. 2 suggests that the exciton transition of PbMoO<sub>4</sub> is also attributed to the cationic excitation as in the case of PbWO<sub>4</sub>. In the scheelite structure, a Pb<sup>2+</sup> ion is at the site of S<sub>4</sub> symmetry surrounded by eight O<sup>2-</sup> ions. The Pb 6p state splits into the  $\Gamma_{3,4}$  level and the  $\Gamma_2$  level due to the uniaxial crystal-field along the *c*-axis. The band 1 observed for **E**//*a* and the band 2 for **E**//*c* are ascribed to the transitions from the top of the valence band of the  $\Gamma_1$  level to the  $\Gamma_{3,4}$  level and the  $\Gamma_2$  level, respectively. The splitting of the peaks *a*<sub>1</sub> and *a*<sub>2</sub> of the band 1 originates from the spin-orbit splitting of the Pb 6p state.

On the other hand, some differences are also observed between the spectra of both materials. The intensity of the peak *a*<sub>1</sub> is stronger than that of *a*<sub>2</sub> in

PbWO<sub>4</sub>, and vice versa in PbMoO<sub>4</sub>. In PbWO<sub>4</sub>, peaks *c*<sub>1</sub> and *c*<sub>2</sub> are observed clearly, while no appreciable structure is seen on the weak plateau in the 3.4–4.0 eV region for **E**//*c* in PbMoO<sub>4</sub>. According to the theoretical calculation [2], the magnitudes of the contribution of Pb state to the top of the valence band and the bottom of the conduction band of PbMoO<sub>4</sub> are about 0.7 times as small as those of PbWO<sub>4</sub>. It is supposed that the difference in magnitudes of the contribution of Pb state is responsible for the different features of the exciton band of PbMoO<sub>4</sub> and PbWO<sub>4</sub> [3].

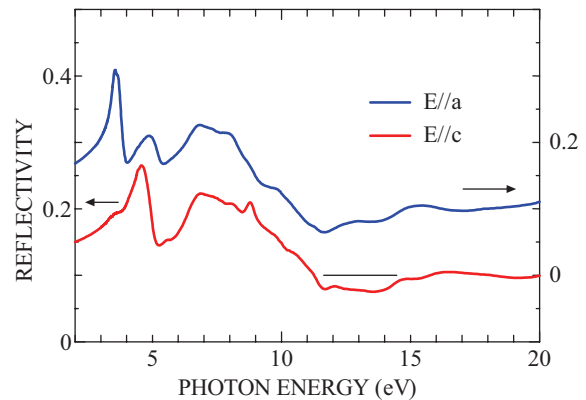


Fig. 1. Reflectivity spectra of PbMoO<sub>4</sub> at 6 K for **E**//*a* and **E**//*c*.

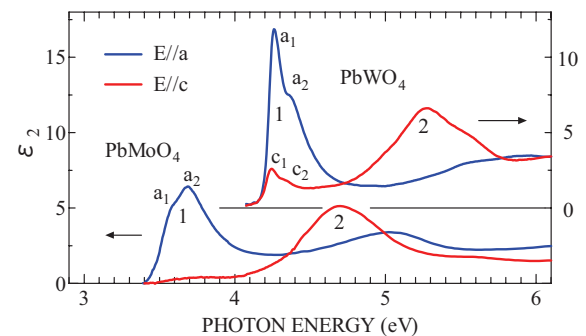


Fig. 2. Imaginary part of the dielectric function of PbMoO<sub>4</sub> and PbWO<sub>4</sub> for **E**//*a* and **E**//*c* in the region below 6 eV.

[1] M. Fujita *et al.*, Phys. Rev. B **65** (2002) 195105.

[2] M. Itoh *et al.*, J. Phys. Soc. Jpn. **75** (2006) 084705.

[3] M. Fujita *et al.*, Phys. Status Solidi B **247** (2010) 405.

# Identification of Cr<sup>3+</sup> Impurity in LaAlO<sub>3</sub> by Photoluminescence

E. Hirata and Y. Ohki

Dept. Electrical Engineering and Bioscience, Waseda University, Shinjuku 169-8555, Japan

Lanthanum aluminate (LaAlO<sub>3</sub>) has been attracting much attention as a promising candidate for a gate insulator in advanced metal-oxide-semiconductor devices. By analyzing photoluminescence (PL) properties of LaAlO<sub>3</sub>, we have been examining presence of localized states in the band gap, which may induce leakage current.

## Experimental

The samples examined are LaAlO<sub>3</sub> (100) single crystals grown by the Czochralski method and LaAlO<sub>3</sub> thin films prepared by a spin-coating method. The films were annealed in oxygen at designated temperatures between 600 and 1000 °C. Using synchrotron radiation under multibunch operation at the BL1B line of UVSOR Facility as a photon source, PL spectra were measured at 10 K. Crystallization of thin films were confirmed by in-plane X-ray diffraction (XRD) measurements.

## Results and Discussion

Figure 1(a) shows PL spectra induced by 6.4-eV photons, obtained at 10 K for the crystal and the films deposited and annealed on Si monocrystal substrates. The films annealed at 600 and 700 °C have no PL peaks, while those annealed at 800, 900, and 1000 °C and the crystal sample have three sharp PL peaks at about 1.60, 1.64, and 1.68 eV. Figure 1(b) shows PL spectra similarly obtained for the films deposited on CaF<sub>2</sub> monocrystal substrates. When the films were annealed at 800 °C or higher, three PL peaks appear similarly to the films on the Si substrates, but at much higher energies, namely at 1.86, 2.00, and 2.14 eV.

The XRD patterns shown in Fig. 2 indicate that the films annealed at 800 °C or higher are polycrystalline, while those annealed at 600 and 700 °C are amorphous. Comparison of XRD spectra between the two annealed polycrystalline films on the Si and CaF<sub>2</sub> substrates indicates that the lattice constant is smaller if substrate is CaF<sub>2</sub>.

It is known that the luminescence due to Cr<sup>3+</sup> in Al<sub>2</sub>O<sub>3</sub> appears only when the sample is crystalline [1]. This is due to energy state splitting of *d* orbitals in Cr<sup>3+</sup> by the crystal field [2]. Furthermore, the PL spectral shapes observed in the single crystal samples and polycrystalline films on the Si substrate in the present study and those of R lines of Cr<sup>3+</sup> in LaAlO<sub>3</sub> are similar [3]. Therefore, there is a possibility that the present LaAlO<sub>3</sub> samples contain Cr<sup>3+</sup> ions as an impurity. Since the energy state of Cr<sup>3+</sup> ions is significantly influenced by the crystal field [2], the difference in PL peak energy among the samples deposited on different substrates should be due to the lattice distortion.

The authors bought the single crystals and

chemicals for making thin films from different companies. Furthermore, it is known that Al<sub>2</sub>O<sub>3</sub> often contains Cr<sup>3+</sup> ions as an impurity [1,4]. Therefore, there is a high possibility that the raw material or ore of Al contains chromium as an impurity. Detection of Cr<sup>3+</sup> ions by inductively coupled plasma optical emission spectrometry (ICP-OES) failed, indicating that the Cr<sup>3+</sup> content in the present samples is below 1 ppm.

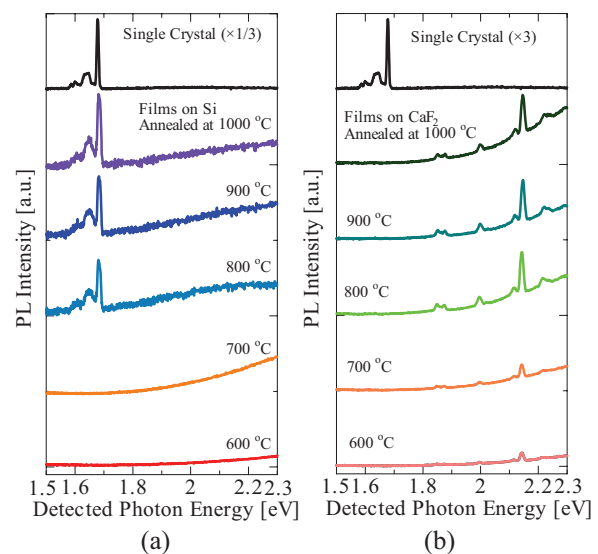


Fig. 1. Comparison of PL spectra induced by 6.4-eV photons, obtained at 10 K in film samples deposited on Si substrates (a) and on CaF<sub>2</sub> ones (b). The PL spectrum obtained in the crystal sample is also shown in each figure (a, b).

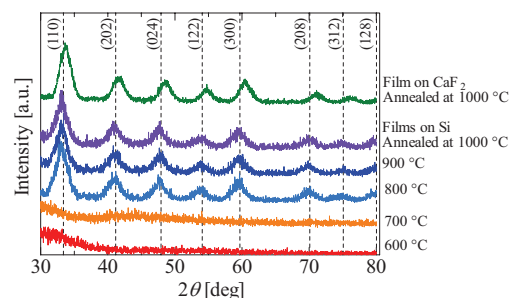


Fig. 2. In-plane XRD patterns of LaAlO<sub>3</sub> film samples.

- [1] J. Kakoš *et al.*, *J. Sol-Gel Sci. Technol.* **21** (2001) 167.
- [2] S. Xia *et al.*, *Phys. Rev. B* **35** (1987) 7671.
- [3] J. Heber *et al.*, *Z. Phys.* **246** (1971) 261.
- [4] T.-P. Lee *et al.*, *J. Vac. Sci. Technol. B* **22** (2004) 2295.

## Photoluminescence from a Bundle of Single-Walled Carbon Nanotubes

M. Itoh, T. Kajitani and H. Mitani

*Department of Electrical and Electronic Engineering, Shinshu University, Nagano 380-8553, Japan*

The observation of photoluminescence (PL) from single-walled carbon nanotubes (SWNTs) underlines their enormous and promising potential for photonic and optoelectronic applications. The PL is ascribed to the radiative decay of free excitons (FEs).

In practical growth condition, about one-third of all possible SWNTs exhibit metallic properties and the remaining two-third act as semiconductors. Therefore, there is a broad consensus [1, 2] that, if one wants to observe the PL from SWNTs, a semiconducting SWNT should be spatially isolated, because the bundling leads to rapid energy transfer to metallic SWNTs where the FEs decay nonradiatively. This consensus, however, neglects an inviting possibility that the FEs can emit PL before the energy transfer takes place, because they have finite lifetimes. In the present study, we have examined whether this possibility is ruled out or not.

### Experiment

HiPco-grown SWNTs (CNI; USA) were dispersed in ethanol with the help of a homogenizer. By spraying the nanotube suspension onto a freshly cleaved BaF<sub>2</sub> crystal, homogeneous SWNT film with a thickness of about 10<sup>-5</sup> cm was prepared. PL was observed by an Acton SpectraPro300i monochromator equipped with a liquid-nitrogen cooled ICCD camera. This detection system has suitable sensitivity in the wavelength range  $\lambda_m = 200\text{--}1000$  nm, with a spectral resolution of 10 nm. The excitation wavelength  $\lambda_{ex}$  was changed in 2 nm steps with a resolution of 0.5 nm, and for each step the emission spectrum was integrated over 300 sec. Although as-made and aged films were examined, no clear difference was found between both results. Morphological information of the new film was obtained by using a digital microscope VHX-1000 (Keyence).

### Results and Discussion

Figure 1 shows a microscope image ( $\times 5000$ ) of the as-made film investigated in this study. From the figure, it is obvious that our sample consists of a bundle of well-dispersed SWNTs.

In Fig. 2 is presented the contour plot of the three-dimensional emission-excitation spectrum of our SWNTs measured at a temperature  $T = 5$  K. An emission band peaking at  $\lambda_m \approx 950$  nm is clearly observed. This emission is excited in the range of  $\lambda_{ex} > 590$  nm. Judging from these spectral characteristics, we likely attribute the 950 nm emission peak to the radiative recombination of FEs in STWNs with (8, 3)

chiral index [1, 2]. Of course, only a small part of FEs could decay in semiconducting SWNTs by emitting PL. From the present observation, however, it is supposed that the coherent length of energy transfer is not so long as one has predicted so far.

The emission intensity of the 950 nm peak was nearly temperature-independent in the range  $T = 5\text{--}300$  K, which suggests that the coherent length is not so sensitive to the temperature.

The authors would like to thank Mr. Y. Aihara of Keyence Co. for his help in the observation of microscope images of our sample. This work was supported by the CLUSTER (the second stage) of the Ministry of Education of Japan.

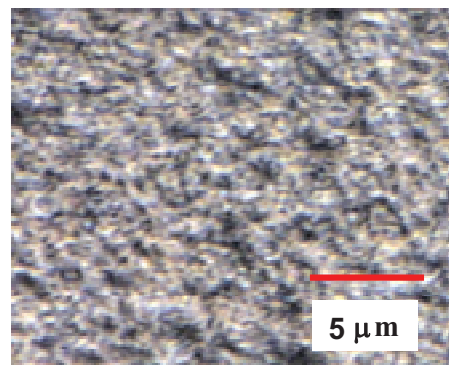


Fig. 1. Microscope image ( $\times 5000$ ) of an as-made SWNT film investigated in the present study.

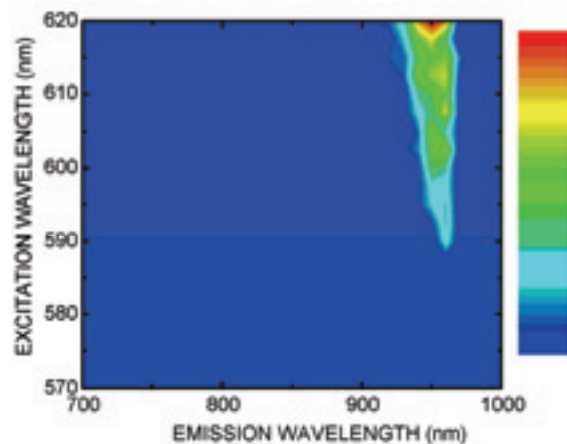


Fig. 2. Contour plot of the three-dimensional emission-excitation spectrum of a bundle of SWNTs dispersed on a BaF<sub>2</sub> substrate measured at  $T = 5$  K.

[1] S. M. Bachilo, *et al.*, *Science* **298** (2002) 2361.

[2] P. H. Tan, *et al.*, *Phys. Rev. Lett.* **99** (2007) 137402.

## Optical Study of the Insulator-Metal Transition in $R_{2-x}\text{Sr}_x\text{NiO}_4$

M. Uchida<sup>1</sup>, J. Fujioka<sup>2</sup>, Y. Kaneko<sup>2</sup>, Y. Onose<sup>1,2</sup> and Y. Tokura<sup>1,2,3</sup>

<sup>1</sup>*Department of Applied Physics, University of Tokyo, Tokyo 113-8656, Japan*

<sup>2</sup>*Multiferroics Project, ERATO, Japan Science and Technology Agency (JST), Tokyo 113-8656, Japan*

<sup>3</sup>*Cross-Correlated Materials Research Group (CMRG), ASI, RIKEN, Wako, Saitama 351-0198, Japan*

Insulator-metal transition in strongly correlated electron systems has attracted great attention in the field of condensed matter physics [1]. It results in the reconstruction of the electronic structure on a large energy scale of several eV accompanying the changes of charge/spin/orbital states. Optical spectroscopy is one of the most powerful probes for investigating the change of high-energy electronic states systematically and provides the essential information for understanding the multi-degree-of-freedom coupled phenomena.

During this beam time, we measured the in-plane reflectivity spectra for layered perovskite nickelates  $R_{2-x}\text{Sr}_x\text{NiO}_4$  ( $R$ : rare earth element) in an energy region between 4 and 42 eV at room temperature using the beam line BL1B. We obtained the optical conductivity spectra by the Kramers-Kronig analysis of the measured spectra connected to the lower-energy ones.  $R_{2-x}\text{Sr}_x\text{NiO}_4$  is a typical two-dimensional insulator-metal transition system. While diagonal-stripe charge-spin ordering and checkerboard charge ordering are discerned around  $x \sim 1/3$  and  $x \sim 1/2$ , respectively, the insulator-metal transition occurs at  $x \sim 1$  accompanying the melting of the charge ordered state [2, 3].

First, we discuss the overall features of the high-energy electronic states. Figure 1 shows the optical conductivity of  $\text{Nd}_{2-x}\text{Sr}_x\text{NiO}_4$  ( $x=1.0$ ) in the energy range 0-35 eV at room temperature. It is noted that several peaks are observed in the spectrum. Previous optical study reported similar spectra for other layered perovskites  $\text{La}_{2-x}\text{Sr}_x\text{MO}_4$  ( $M = \text{Cr, Mn, Fe, and Co, } x=1.0$ ). The authors could successfully assign the origin of the peaks based on the systematic  $M$ -dependent energy shift [4]. Comparing our data

with them, three peaks above 10 eV (A, B, and C) can be assigned to  $\text{Nd}4p \rightarrow \text{Nd}5d$ ,  $\text{Sr}4p \rightarrow \text{Sr}4d$ , and  $\text{O}2s \rightarrow \text{Ni}3d$  excitations, respectively. We also assign two peaks D and E to the transitions from the  $\text{O}2p$  band to some higher-lying conduction bands. The broad peak indicated by the solid triangle is remnant of the charge transfer (CT) gap excitation. The small CT gap compared with the other layered perovskites implies the instability of the insulator-metal transition for  $M=\text{Ni}$  (except the superconducting transition for  $M=\text{Cu}$ ).

Next, we focus on the doping variation of the electronic structure in the course of the insulator-metal transition. In Fig. 2, we show the low-energy optical conductivity spectra of  $\text{Nd}_{2-x}\text{Sr}_x\text{NiO}_4$  ( $x=0.5-1.3$ ) at 10K. The magnitude of the gap rapidly decreases with hole doping from  $x=0.5$ , reflecting the melting of the checkerboard-type charge order. While the gap is almost closed around  $x=1.0$ , a conspicuous peak structure is observed around 0.2 eV, indicating the incoherent transport caused by the strong charge correlation. In the higher doping range ( $x=1.3$ ), the peak shifts to the lower energy and is merged to Drude response. Thus, we show in terms of optical spectra that the checkerboard type charge correlation dominates the charge dynamics near the insulator-metal transition in this system.

- [1] M. Imada *et al.*, Rev. Mod. Phys. **70** (1998) 1039.  
 [2] S. Shinomori *et al.*, J. Phys. Soc. Jpn. **71** (2002) 705.  
 [3] K. Ishizaka *et al.*, Phys. Rev. B **67** (2003) 184418.  
 [4] Y. Moritomo *et al.*, J. Phys. Soc. Jpn. **64** (1995) 4117.

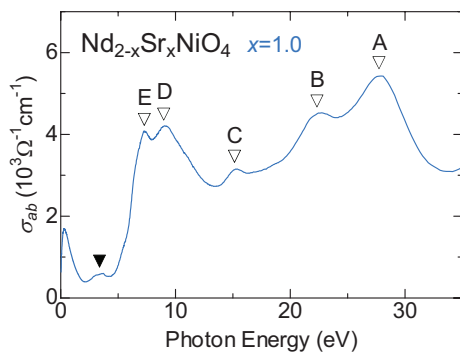


Fig. 1. Optical conductivity spectrum of  $\text{Nd}_{2-x}\text{Sr}_x\text{NiO}_4$  ( $x=1.0$ ) over wide energy region at room temperature.

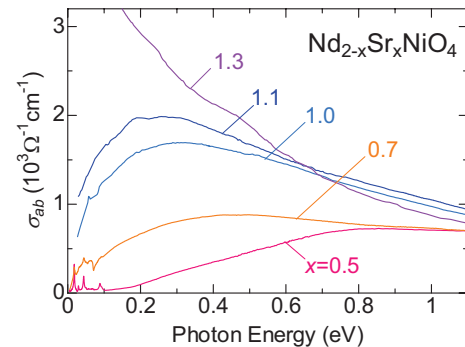


Fig. 2. Doping variation of the in-plane optical conductivity of  $\text{Nd}_{2-x}\text{Sr}_x\text{NiO}_4$  ( $x=0.5-1.3$ ) at the lowest temperature, 10K.

## Soft X-Ray Spectroscopy of DNA Duplexes

H. Yamane<sup>1</sup>, W. Hua<sup>2</sup>, H. S. Kato<sup>3</sup>, T. Hatsui<sup>4</sup>, M. Kawai<sup>3,5</sup>, Y. Luo<sup>2</sup>, H. Ågren<sup>2</sup> and N. Kosugi<sup>1</sup>  
<sup>1</sup> Institute for Molecular Science, Okazaki 444-8585, Japan

<sup>2</sup> Dept of Theoretical Chemistry, Royal Institute of Technology, S-106 91 Stockholm, Sweden

<sup>3</sup> The Institute of Physical and Chemical Research (RIKEN), Wako 351-0198, Japan

<sup>4</sup> XFEL Project Head Office, RIKEN & JST-PREST, Hyogo 679-5148, Japan

<sup>5</sup> Dept of Advanced Materials Science, University of Tokyo, Kashiwa 277-8501, Japan

### Introduction

The electronic structure and its properties in DNA polymers have received great attention for possible molecular nanoelectronics since the discovery of the double helix structure of DNA. In the present work, we have undertaken experimental and theoretical study of soft X-ray spectroscopies for DNA base pairs, that is, fluorescence yield X-ray absorption (FY-XAS) and X-ray emission (XES) spectroscopies applied to poly(dA)-poly(dT) (AT) and poly(dG)-poly(dC) (GC) DNA duplexes. We have found that the stacking of pairs has very little influence on the spectra. The X-ray spectra of a DNA composed by mixed Watson-Crick base pairs are well reproduced by linear combinations of base pairs involved, and the amine and imine nitrogens show noticeable differences as building blocks in the FY-XAS and XES spectra [1].

### Experiment

We prepared thick films of AT- and GC-DNA. These duplexes were diluted with deionized water (17.8 MΩ·cm) to a concentration of 1.25 mg/ml. The solutions were casted on the SiO<sub>2</sub>/p-Si(111) substrates. The film thickness is about 100–200 nm. These samples are almost the same as those measured at the previous resonant photoemission experiments [2].

The FY-XAS and XES experiments were performed at BL3U. The FY-XAS spectra were measured by the highly efficient fluorescence-yield method using an MCP assembly with the center hole (F2223-21SH, Hamamatsu Photonics K.K.). The XES spectra were measured using a transmission-grating spectrometer. All measurements were performed at 300 K. In order to avoid the radiation damage of the sample during the measurements, the X-ray beam spot on the sample was continuously moved by scanning the sample.

### Results and Discussion

Figure 1 shows a set of the N K-edge FY-XAS spectrum and the excitation energy ( $h\nu$ ) dependence of the N K $\alpha$  XES spectra for the AT-DNA film. One finds in the XES spectra that the spectral difference between the imine ( $-N=$ ) and amine ( $-NH-$ ) groups can be distinguished; the resonance photoabsorption for the imine nitrogens appears at  $h\nu = 399.4$  eV, while that for the amine nitrogens appears at a higher  $h\nu = 401.6$  eV. At the imine site, the resonant XES spectrum has two prominent features; one shoulder at  $h\nu = 390$  eV and one peak at  $h\nu = 393$  eV. At the amine site, in contrast, the peak structure appears at

different photon energy ( $h\nu = 394$  eV) with weak intensity as compared to that appears at the imine site. From the theoretical calculation [1], we found that the effect of stacking between pairs is of little consequence for the experimental XES spectra and that these with a good approximation can be represented just by one of its constituting base pairs with the hydrogen-bonding interaction.

Furthermore, one can find that the elastic peak in the XES spectra shows an asymmetric lineshape with a low-energy tail structure. The intensity of this tail structure depends on  $h\nu$ ; in particular at the imine site, the tail structure is more intense. This tail structure may originate from the recombination emission [3] due to the fast motion of hydrogen bonded protons between the pairs, which depends on the degree of localization of the excited state. The observation of the tail structure indicates that the excited  $\pi^*$  state at the imine site is strongly localized, which agrees well with the scenario of a charge hopping transport in DNA duplexes proposed by the previous resonant photoemission work [2].

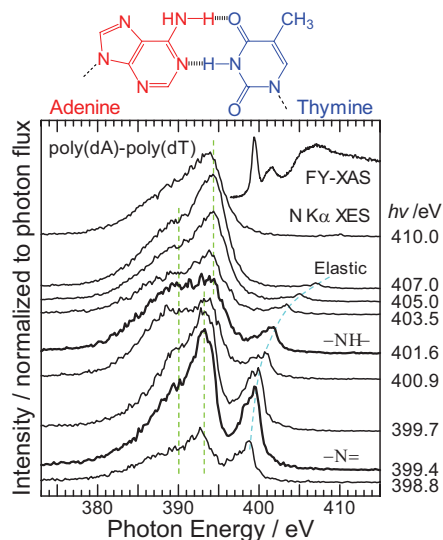


Fig. 1. Set of the N K-edge FY-XAS spectrum and the N K $\alpha$  XES spectra for the AT-DNA film. The molecular structure of adenine and thymine, included in the AT-DNA, at the configuration of the hydrogen-bonding interaction are also shown.

[1] W. Hua *et al.*, J. Phys. Chem. C, submitted.

[2] H.S. Kato *et al.*, Phys. Rev. Lett. **93** (2004) 086403.

[3] Y. Ma *et al.*, Phys. Rev. Lett. **71** (1993) 3725.

# Local Intermolecular Interaction in $\alpha$ -Crystalline Films of Zinc-Phthalocyanine Studied by Soft X-Ray Emission Spectroscopy

H. Yamane<sup>1</sup>, T. Hatsui<sup>2</sup> and N. Kosugi<sup>1</sup>

<sup>1</sup> Institute for Molecular Science, Okazaki 444-8585, Japan

<sup>2</sup>XFEL Project Head Office, RIKEN & JST-PREST, Hyogo 679-5148, Japan

## Introduction

The photon-in/photon-out technique of X-ray emission spectroscopy (XES) measures X-rays emitted as a resonant Raman scattering or decay process of the inner-shell excitation, which gives information about element-specific excitations and occupied partial density of states (pDOS) of unionized and ionized materials. This technique has no restriction about samples and its atmospheres, and moreover, it is known as bulk sensitive methods (typically, hundreds of nm for soft X-rays).

In this work, we investigated the local electronic structure of Zn-phthalocyanine (ZnPc), which is one of the promising materials for organic photovoltaics. In order to study the local intermolecular interaction in ZnPc solids, we prepared the crystalline and amorphous films of ZnPc. We found a distinct crystalline structure dependence in the resonant XES (RXES) spectra, which can be originated from the site-specific intermolecular interaction.

## Experiment

The ZnPc sample was prepared by the vacuum evaporation onto the naturally oxidized *p*-Si(111) surface. The deposition amounts of 400 nm and deposition rate of 1 nm/min were measured with a quartz crystal microbalance. The crystalline ZnPc film was obtained at the substrate temperature during the deposition of 340 K, while the amorphous ZnPc film was obtained at 84 K. The crystallinity of these ZnPc films at the room temperature of 300 K was confirmed by X-ray absorption spectroscopy (XAS) and by X-ray diffraction (XRD).

The XES measurements were performed by using a transmission grating spectrometer at BL3U of the UVSOR facility [1]. The incident soft X-ray beam was focused to 40  $\mu\text{m}$  (horizontal)  $\times$  20  $\mu\text{m}$  (vertical) at the sample position. All XES measurements were performed at 300 K. For the XES spectra, we need a small photon spot size and long accumulation times of 60–90 min per 1 spectrum. Even in the photon flux of  $10^{11}$  photons/sec range, the XES spectra of ZnPc films show the evidence for the radiation damage within 10–15 min X-ray irradiation. In order to avoid the radiation damage, the X-ray irradiated spot was continuously moved by scanning the sample at the rate of 20  $\mu\text{m}/\text{min}$  during the measurements.

## Results and Discussion

Judging from the XRD and XAS results (not shown), the ZnPc molecules, deposited at the 340 K

substrate temperature, form an ordered  $\alpha$ -crystalline structure where the molecular plane is tilted of about  $70^\circ$  with respect to the substrate surface, while the molecules deposited at 84 K form an amorphous structure.

The normal XES spectra, which reflect the occupied pDOS, do not show the clear difference between the crystalline and amorphous film (not shown). On the other hand, as shown in Fig. 1, the distinct crystalline structure dependence was observed in the RXES spectra. The elastic peak in the C  $K\alpha$  RXES shows a symmetric lineshape for both the crystalline and amorphous films, but the elastic peak in the N  $K\alpha$  RXES shows an asymmetric lineshape for the crystalline film, while the amorphous film gives the symmetric elastic peak, which is the indication of the presence of the Raman active intermolecular interaction at the N site in the crystalline film. As the origin of the asymmetric elastic peak, the vibronic excitation that accompanies direct recombination emission [2] can be considered. In this context, the broad peak around 0–1 eV in the recombination emission suggests the higher degree of localized character of the  $\pi^*$  states as compared to the case of graphite [2] and DNA molecules [3].

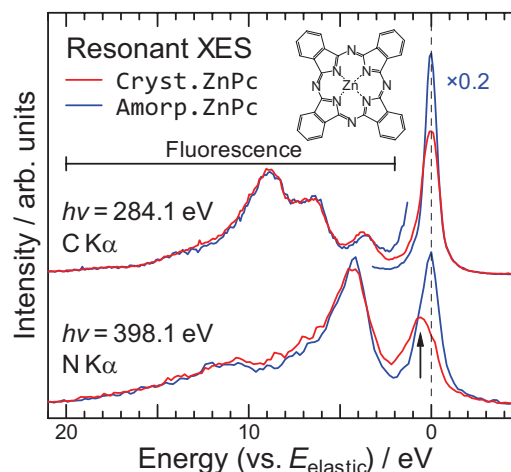


Fig. 1. The C  $K\alpha$  and N  $K\alpha$  resonant XES spectra of crystalline and amorphous films of ZnPc. The C  $K\alpha$  and N  $K\alpha$  excitation energies  $h\nu$  were set to the first C K and N K resonance peaks in XAS.

- [1] T. Hatsui *et al.*, J. Electron Spectrosc. Relat. Phenom. **144-147** (2005) 1059.
- [2] Y. Ma *et al.*, Phys. Rev. Lett. **71** (1993) 3725.
- [3] H. Yamane *et al.*, a separate page in this volume.

## Dilute Multi Ferroic Semiconductor GaCrN-II

S. Emura<sup>1</sup>, H. Tambo<sup>1</sup>, K. Higashi<sup>1</sup> and K. Fukui<sup>2</sup>

<sup>1</sup>ISIR, Osaka University, Ibaraki 567-0047, Japan

<sup>2</sup>Faculty of Engineering, University of Fukui, Fukui 910-8507, Japan

Semiconductor systems with a wurtzite structure carrying a small amount of transition metals sometimes show the various physical properties. GaN:Cr is one of those. This substance exhibits magnetism and ferro-electrics. Therefore, we can expect to observe the anisotropic phenomena. The specimens studied here are single crystals in the thin layer form on a MgO and an Al<sub>2</sub>O<sub>3</sub> substrate. On the MgO substrate, the crystal constructs the cubic structure (zinc-blende structure) and grows with a wurtzite structure on the Al<sub>2</sub>O<sub>3</sub> substrate.

Figure 1 exhibits the incident angle dependence of the absorption spectra of the crystal with the wurtzite structure and CrN with rock salt structure for the reference in VUV region observed at BL4B at UVSOR. At zero angles, the electric field of incident photon is vertical to the crystal c-axis of GaN:Cr. The absorption band around 28 nm (44.3 eV), which is tentatively assigned to the transition from 3p of the Cr atom to the s-like conduction band of matrix because of the wide half width, strongly depends on the direction of the electric polarization of the incident photon. In the parallel electric field to the c-axis, the band vanishes, indicating anisotropy along the c-axis. As the XAFS analysis of these specimens predicts the spontaneous elastic deformation (quasi Jahn – Teller effect) involving the local electric polarization, this finding is an evidence of the ordering of the deformation and consequent electric polarization.

Figure 2 present the linear dichroism spectra for the cubic GaN:Cr in X-ray energy region. Here, the intensity of the spectra is normalized at the end (6030 eV) of the spectra shown in the figure. A clear doublet peak in the pre-edge region, which is assigned to the transition from 1s to 3d, and splits owing to the ligand field, can be found. The lower peak of the doublet exhibits the explicit linear dichroism. The observation indicates the ordering of the deformation in the cubic GaN:Cr also. In conclusion, the both hexagonal and cubic GaN:Cr crystals show the Jahn – Teller deformation around the Cr ions and the deformation is in ordering.

The detailed VUV and X-ray excitation spectra are observed. The strong angular dependence of the peak around 28 nm and linear dichroism at 5988 eV are found. This observation of the dichroism in GaN:Cr with the cubic structure indicates that the CrN<sub>4</sub> tetrahedron in the local coordination at the Cr ion suffers deformation. The Cr ions may shift slightly from the lattice center. it is apparent from the figures that the local spontaneous electric polarization is

induced around the doped Cr ion. Here, it should be noticed that there are four nearly equivalent legs because the original site symmetry is nearly T<sub>d</sub>, and we cannot distinguish these four legs from the XAFS analysis. The parallel shifts may randomly be distributed in the matrix or ordered along some direction of the matrix.

The GaN:Cr is one of the dilute magnetic semiconductors. From our observation, it behave as a ferro-electric and elastic material. The coupling among those may lead to substances of a new category in multi-ferroic research field.

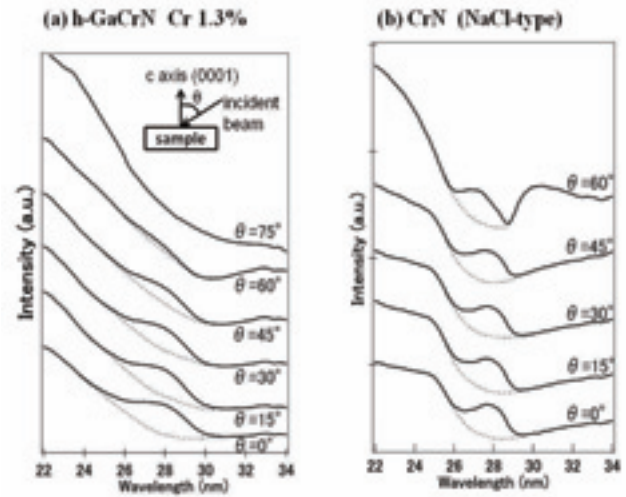


Fig. 1. Angular dependence of the absorption spectra.

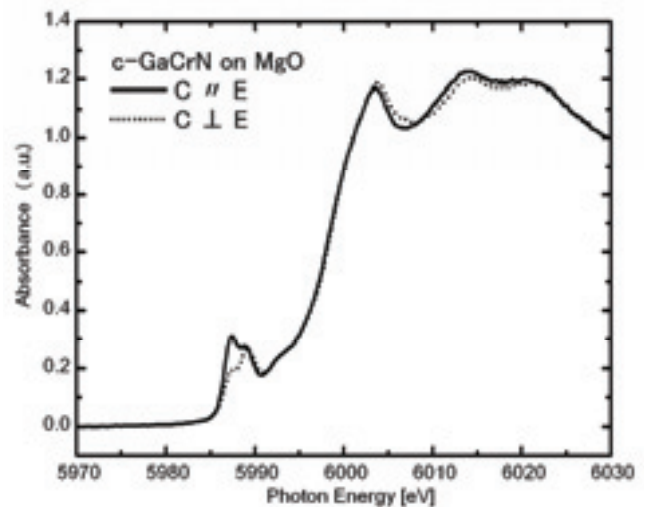


Fig. 2. Linear dichroism spectra in X-ray energy region.

## Charge State Analysis of Mn Ions in $\text{Pr}_{1-x}\text{Ca}_x\text{MnO}_{3-\delta}$ by Mn-L<sub>2,3</sub> XANES Spectra

H. Kanamori, T. Yoshioka and T. Yamamoto

*Faculty of Science and Engineering, Waseda University, Shinjuku 169-8555, Japan*

$\text{Pr}_{1-x}\text{Ca}_x\text{MnO}_{3-\delta}$  has been extensively studied, because it has unique electronic and magnetic properties such as colossal magnetoresistance and metal-insulator transition [1]. In order to understand such properties, it is essential to know the charge state, i.e., valence, of Mn ions in these materials. There are two scenarios to compensate the system; i) valence of Mn ions control the system, i.e., from  $\text{Mn}^{3+}$  to  $\text{Mn}^{4+}$ , ii) oxygen vacancy is created, when Ca is incorporated into  $\text{PrMnO}_3$ . However, these mechanisms have not yet been understood. Then we have performed the charge state analysis of Mn ions in  $\text{Pr}_{1-x}\text{Ca}_x\text{MnO}_{3-\delta}$  by the Mn-L<sub>2,3</sub> X-ray absorption near-edge structure (XANES) measurements.

$\text{Pr}_{1-x}\text{Ca}_x\text{MnO}_{3-\delta}$  samples are synthesized by the conventional solid-state reaction method. Mn-L<sub>2,3</sub> XANES spectra were observed at BL4B in UVSOR by the total electron yield (TEY) method. The incident beam was monochromatized with a grating (800 lines/mm) double crystal monochromator.

Prior to XANES analysis, all the samples were characterized by the X-ray diffraction (XRD).  $\text{Pr}_{1-x}\text{Ca}_x\text{MnO}_{3-\delta}$  crystallizes perovskite structure at ambient condition. No extra peaks can be found in the observed XRD patterns except for those of the perovskite structured  $\text{Pr}_{1-x}\text{Ca}_x\text{MnO}_{3-\delta}$ .

Observed Mn-L<sub>3</sub> XANES spectra of the samples here synthesized are shown in Fig. 1. Valences of Mn ions in  $\text{PrMnO}_3$  and  $\text{CaMnO}_3$  are 3+ and 4+, respectively, when it is assumed that there is no oxygen vacancy in these materials. Spectral profiles of Mn-L<sub>3</sub> XANES spectra of these two materials show significant difference. Those of  $\text{Pr}_{1-x}\text{Ca}_x\text{MnO}_{3-\delta}$  with  $x=0.3, 0.4, 0.5$  changes from the shape of  $\text{Mn}^{3+}$  to  $\text{Mn}^{4+}$  as increment of Ca concentration. These experimental results suggest that valence of Mn ions in  $\text{Pr}_{1-x}\text{Ca}_x\text{MnO}_{3-\delta}$  changes continuously as increment of Ca concentration.

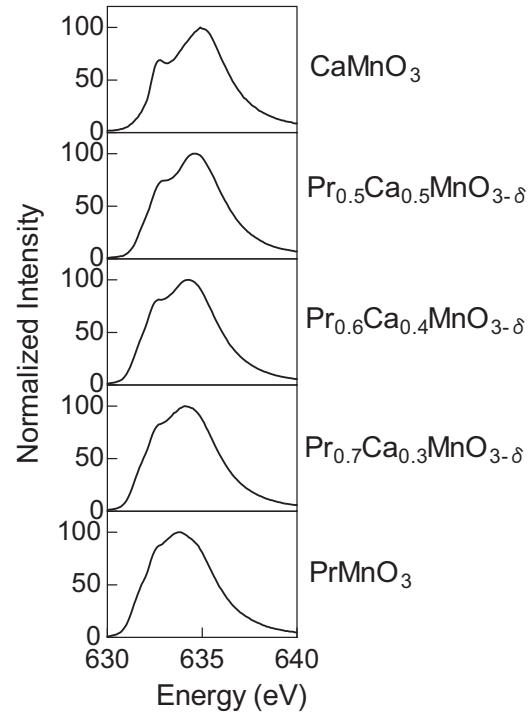


Fig. 1. Observed Mn-L<sub>3</sub> XANES spectra of  $\text{Pr}_{1-x}\text{Ca}_x\text{MnO}_{3-\delta}$ .

[1] Y. Tokura and N. Nagaosa, *Science* **288** (2000) 462.

## Three-Dimensional Angle-Resolved Photoemission Study on $\text{EuFe}_2\text{As}_2$

T. Hajiri<sup>1</sup>, R. Niwa<sup>2</sup>, S. Murakami<sup>2</sup>, H. Miyazaki<sup>3</sup>, J. B. Hong<sup>4</sup>, Y. R. Jang<sup>4</sup>, S. Kimura<sup>3,5</sup>,  
Y. S. Kwon<sup>4</sup> and T. Ito<sup>1,6</sup>

<sup>1</sup>Graduated School of Engineering, Nagoya University, Nagoya 464-8603, Japan

<sup>2</sup>School of Engineering, Nagoya University, Nagoya 464-8603, Japan

<sup>3</sup>UVSOR Facility, Institute for Molecular Science, Okazaki 444-8585, Japan

<sup>4</sup>Department of Physics, Sungkyukwan University, Suwon 440-749, Korea

<sup>5</sup>School of Physical Sciences, the Graduate University for Advanced Studies (SOKENDAI),  
Okazaki 444-8585, Japan

<sup>6</sup>Nagoya University Synchrotron Radiation Research Center, Nagoya University, Nagoya  
464-8603, Japan

Iron pnictides superconductor discovered recently has been intensively studied both from experiment and theory, however an essential mechanism of its anomalous superconductivity has not been clarified yet. To understand the mechanism of superconductivity, the superconducting gap information, i.e., the origin of superconducting pairing, is one of the most important issues.

To clarify the fundamental electronic structure of Iron pnictides, especially of '122' series, we have performed angle-resolved photoemission spectroscopy (ARPES) on  $\text{EuFe}_2\text{As}_2$  in the heavily underdoped regime where the spin density wave (SDW) formation at  $T_{\text{SDW}}=190$  K as well as an antiferromagnetic transition at  $T_{\text{N}}=20$  K has been expected [2].

Figure 1 (a) and (b) shows momentum distribution curves (MDC) at  $E_{\text{F}}\pm 50$  meV together with the experimental band structure along  $\Gamma\text{X}$  and  $\text{ZR}$ , respectively, obtained by plotting the second-derivative intensity of ARPES spectra of  $\text{EuFe}_2\text{As}_2$  at 30 K. We have found two and one hole-like FS's around  $\Gamma$  and Z points, respectively, while the band structure calculation on the '122' series  $\text{BaFe}_2\text{As}_2$  expects one and two hole-like FS's around the  $\Gamma$  and Z points [3] in against to the present ARPES result.

Furthermore, from the inter-plane FS along  $k_z$ -direction (Fig. 2) obtained by utilizing the photon energy dependent ARPES on the same sample  $\text{EuFe}_2\text{As}_2$  at 30K, we found that the hole-like FS observed around the  $\Gamma$  point has been separated to the two hole-like FS as approaching to the Z point together with the reduction of FS sizes. This suggests that a single hole-like FS pocket around  $\Gamma$  point originating from the combination of two hole-like FS degenerating within our experimental momentum resolution ( $\Delta\theta\sim 0.17^\circ\sim\Delta k\sim 0.011\text{ \AA}^{-1}$  at  $h\nu=38$  eV).

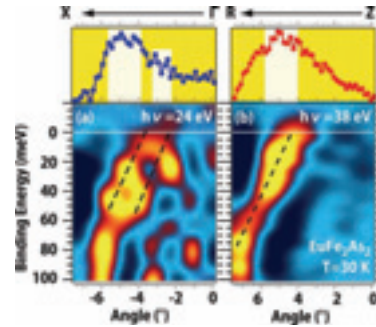


Fig. 1. Band structure along  $\Gamma\text{X}$  (a) and  $\text{ZR}$  (b) axis obtained by plotting the second-derivative intensity of ARPES spectra of  $\text{EuFe}_2\text{As}_2$  with  $h\nu=24$  eV (a) and 38 eV (b), respectively, at  $T=30$  K. Upper panel shows MDC spectrum at  $E_{\text{F}}\pm 50$  meV.

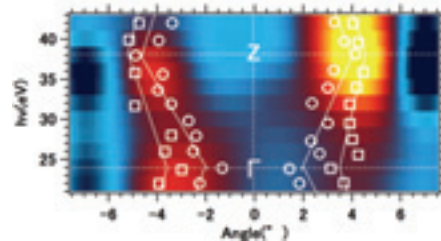


Fig. 2. Fermi surface image on  $\Gamma\text{XRZ}$  plane of  $\text{EuFe}_2\text{As}_2$ . Open circles and squares are the peak positions of MDC spectra at  $E_{\text{F}}$ . Thin lines are guide for the eyes.

[1] Y. Kamihara *et al.*, J. Am. Chem. Soc. **130** (2008) 3296.

[2] H. S. Jeevan *et al.*, Phys. Rev. B **78** (2008) 020503(R).

[3] Walid MALAEB *et al.*, arXiv: **0906** (2009) 1846v1.

## Ce 4d-4f Resonant Angle-Resolved Photoemission Studies on Quantum Criticality in Heavy-Fermion Ce112 Systems

H. J. Im<sup>1</sup>, H. Miyazaki<sup>2</sup>, T. Ito<sup>3</sup>, S. Kimura<sup>2,4</sup>, K. E. Lee<sup>5</sup> and Y. S. Kwon<sup>5</sup>

<sup>1</sup>*Department of Advanced Physics, Hirosaki University, Hirosaki 036-8561, Japan*

<sup>2</sup>*UVSOR Facility, Institute for Molecular Science, Okazaki 444-8585, Japan*

<sup>3</sup>*Graduate School of Engineering, Nagoya University, Nagoya 464-8603, Japan*

<sup>4</sup>*School of Physical Sciences, The Graduate University for Advanced Studies, Okazaki 444-8585, Japan*

<sup>5</sup>*Department of Physics, Sungkyunkwan University, Suwon 440-746, Korea*

We have performed Ce 4d-4f resonant angle-resolved photoemission spectroscopy (rARPES) on CeNiGe<sub>2</sub> and CeNi<sub>0.7</sub>Co<sub>0.3</sub>Ge<sub>2</sub>, whose ground states are antiferromagnetism (AFM) and quantum critical point (QCP), respectively, in the beamline BL5U of UVSOR. In this weakly hybridized regime, Ce 4f-electrons are considered to be highly localized due to the large repulsive Coulomb interaction between f-electrons and the weak hybridization strength between f- and conduction electrons. In addition, the localized character of f-electrons has been a key point to understand QCP. Therefore, the systematic investigation of Ce 4f-character in weakly hybridized regime is inevitable.

Figure (a) shows the high-resolution on-rARPES spectral image of CeNiGe<sub>2</sub>. In order to investigate the momentum-dependence of Kondo resonance (KR) peaks near the Fermi level ( $E_F$ ), the spectra (energy distribution curves, EDCs) are normalized to the intensity of Ce 4f<sup>7/2</sup> peak around -0.3 eV: it is well known that the intensity ratio of Ce 4f<sup>5/2</sup> peak (the tail of KR peak) to Ce 4f<sup>7/2</sup> peak empirically represents the strength of Kondo coupling in angle-integrated photoemission (AIPES) spectra. Near  $E_F$ , the momentum-dependence of Ce 4f<sup>5/2</sup> state is clearly observed. Besides the above Ce 4f-bands, there is another linearly dispersive band from -0.6 eV to  $E_F$  with weak intensity. This band is composed of non-f states and corresponds to conduction band. We find that the intensity of KR peak is largely enhanced where the conduction band crosses  $E_F$  as in CeCoGe<sub>0.8</sub>Si<sub>1.2</sub>, whose ground state is non-magnetism due to large hybridization strength [1]. Such behaviors are also observed in CeNi<sub>0.7</sub>Co<sub>0.3</sub>Ge<sub>2</sub> (not shown here). As a result, we conclude that the character of f-electrons is itinerant across QCP in agreement with the results of AIPES studies of CeNi<sub>1-x</sub>Co<sub>x</sub>Ge<sub>2</sub> [2].

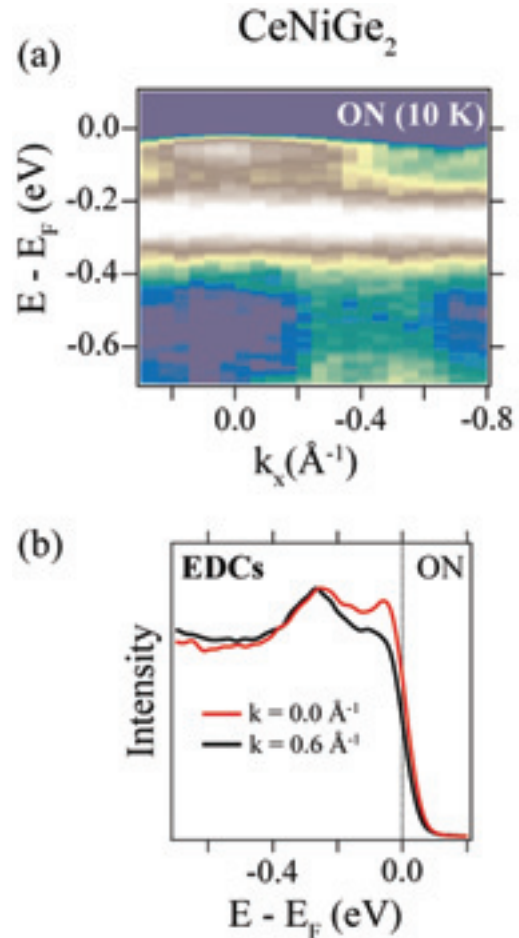


Fig. (a) Ce 4d-4f on-rARPES image of CeNiGe<sub>2</sub> ( $h\nu = 122$  eV,  $T = 10$  K). (b) The energy distribution curves at  $k = 0 \text{ \AA}^{-1}$  (red line) and  $k = 0.6 \text{ \AA}^{-1}$  (black line).

[1] H. J. Im *et al.*, Phys. Rev. Lett. **100** (2008) 176402.

[2] H. J. Im *et al.*, Phys. Rev. B **72** (2005) 220405.

## Temperature-Dependent Photoemission Spectra of Alkanethiolate-Passivated Au Nanoparticles

M. Imamura, T. Fujino, S. Fujimasa and H. Yasuda

*Department of Mechanical Engineering, Kobe University, Kobe 657-8501, Japan*

Metallic nanoparticles attract much attention due to their characteristic properties such as Coulomb blockade, nonlinear optical response, and catalytic activity. In order to elucidate their detailed intriguing properties and to develop the future devices, it is indispensable to understand the electronic structures. In this work, we have carried out the synchrotron-radiation photoemission study of dodecanethiolate-passivated Au nanoparticles supported on the HOPG substrate at various temperatures.

The synthesis procedure of DT-passivated Au nanoparticle is described elsewhere [1]. The synchrotron photoemission study was carried out with the incident photon energy of 190 eV at BL-5U of UVSOR facility.

Figure 1 shows the synchrotron-radiation photoemission spectra of DT-passivated Au nanoparticles with the mean diameter of 2.5 nm in the vicinity of Fermi-level measured at room temperature, 160, and 100 K. The leading edges of the spectra in the vicinity of Fermi-level of all the Au nanoparticles at various temperatures moved away from Fermi-level. Furthermore, the photoemission intensities of the leading edges decrease with decreasing the measurement temperature, and change to the background intensity of HOPG. In our previous work, we have reported that the photoemission spectra in the vicinity of Fermi level of DT-passivated Ag nanoparticles show the deviation from the metallic Fermi-edge, and concluded that these spectra reflect the final-state effect [1, 2]. We have explained the experimental spectra using a theoretical model that takes into account the influence of the photohole remaining on the nanoparticle during the photoemission process and the nanoparticle-substrate interaction. The shift of Fermi edge in the present photoemission spectrum measured at room temperature is well explained by the same picture. Since the final-state effects do not depend on the measurement temperature, the temperature dependence of present photoemission spectra is considered to originate from the change of intrinsic electronic structure of Au nanoparticles. Kubo criterion predicted that the discrete energy states are exhibited when the mean energy-level spacing near Fermi-energy exceeds the characteristic thermal

energy. In the present case, Au nanoparticles at room temperature remain bulk-like electronic structure, since the energy level spacing is narrower than the thermal broadening. With decreasing temperature, the mean energy-level spacing of Au nanoparticles exceeds the characteristic thermal energy. Consequently, Au nanoparticles is expected to have discrete electronic structures. The discrete and low densities of states of Au nanoparticle will lead to decrease the photoemission intensities. From these results it is concluded that the temperature-dependent photoemission spectra in the vicinity of Fermi-level is attributed to temperature-dependent metal-insulator transition that is theoretically predicted.

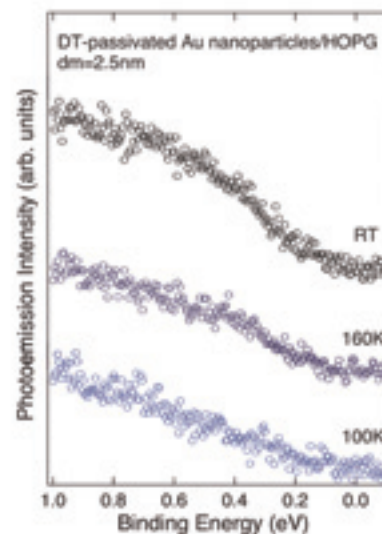


Fig. 1. Synchrotron-radiation photoemission spectra of DT-passivated Au nanoparticles supported on the HOPG substrates in the vicinity of Fermi-level measured with the photon energy of 190 eV at room temperature, 160K, and 100K.

- [1] A. Tanaka, Y. Takeda, M. Imamura and S. Sato, *Appl. Surf. Sci.* **237** (2004) 537-542.  
 [2] M. Imamura and A. Tanaka, *Phys. Rev. B* **73** (2006) 125409-1-125409-5.

BL5U **Detection of Spin-Filtered Surface-States of a Topological Insulator by Polarization Dependent Angle-Resolved Photoemission Spectroscopy**

A. Nishide, F. Nakamura and I. Matsuda

*Institute for Solid State Physics, University of Tokyo, Kashiwa 277-8581, Japan*

The quantum spin Hall (QSH) effect, which makes it possible to produce topologically protected spin currents without magnet, has now attracted interests of researchers in condensed matter physics. Recently, photoemission spectroscopy (PES) studies [1] have mapped band dispersion curves of the surface states of the semiconductor alloy,  $\text{Bi}_{1-x}\text{Sb}_x$  ( $x \sim 0.1$ ), and high-resolution spin-resolved PES measurements [2] have determined their spin orientations between the two time-reversal invariant momenta. These experimental results have clearly indicated a trace of the predicted topological band structure, giving direct evidence of the topological insulator. These previous works have also demonstrated that PES is the most powerful tool for such researches. On the other hand, it has been known that, during the PE process, photoexcitation of electrons with different spin orientations depend on circular polarizations of incident light [3]. Thus, we conducted polarization dependent angle-resolved PES measurements to obtain direct evidence of spin-filtered surface-states of the QSH phase. The experiment was performed at UVSOR BL-5U with the Apple-II type undulator, generating right and left helical light. As shown in Fig., we observed clear variations of photoemission intensity with the circular polarizations. Moreover, we succeeded in detecting two surface-state bands [2],  $\Sigma_2$  and  $\Sigma_1'$ , of the three-dimensional QSH phase at the  $\bar{M}$  point, Fig.(b), confirming the non-trivial topological nature of  $\text{Bi}_{1-x}\text{Sb}_x$  ( $x=0.15$ ).

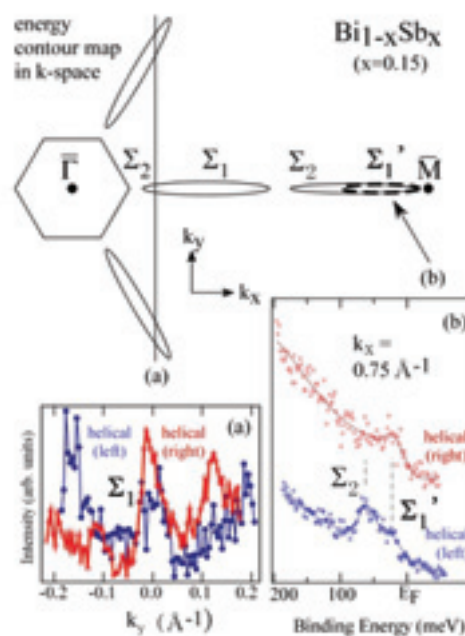


Fig. Schematic drawing of the energy contour map of  $\text{Bi}_{1-x}\text{Sb}_x$  ( $x=0.15$ ) around Fermi level with a series of (a,b) experimental photoemission spectra taken at 20K.

**Acknowledgements**

Alexey A. Taskin and Yoichi Ando in Osaka University are gratefully acknowledged for sample crystals and valuable comments

[1] D. Hsieh *et al.*, Nature **452** (2008) 970.  
 [2] A. Nishide *et al.*, Phys. Rev. B **81** (2010) 041309 (R).  
 [3] M. Mulazzi *et al.*, Phys. Rev. B **74** (2006) 035118.

# Resonance Photoemission Study of Pseudo-One Dimensional Cobalt Oxide $\text{Ba}_3\text{Co}_2\text{O}_6(\text{CO}_3)_{0.7}$

K. Soda<sup>1</sup>, M. Kikuchi<sup>2</sup>, H. Miyazaki<sup>1,3</sup>, M. Inukai<sup>1,4</sup>, M. Kato<sup>1</sup>, S. Yagi<sup>1</sup>,  
K. Iwasaki<sup>1,5</sup> and T. Matsui<sup>1,6</sup>

<sup>1</sup>Graduate School of Engineering, Nagoya University, Nagoya 464-8603, Japan

<sup>2</sup>School of Engineering, Nagoya University, Nagoya 464-8603, Japan

<sup>3</sup>UVSOR Facility, Institute for Molecular Science, Okazaki 444-8585, Japan

<sup>4</sup>Venture Business Laboratory, Nagoya University, Nagoya 464-8603, Japan

<sup>5</sup>Toyota Boshoku Coporation, Kariya 448-8651, Japan

<sup>6</sup>EcoTopia Science Institute, Nagoya University, Nagoya 464-8603, Japan

Recently it has been found that a pseudo-one dimensional  $\text{Ba}_3\text{Co}_2\text{O}_6(\text{CO}_3)_{0.7}$  shows a fairly large thermoelectric power factor of  $0.9 \text{ mWm}^{-1}\text{K}^{-2}$  at 300 K with the thermoelectric power of about  $+120 \mu\text{V K}^{-1}$  and metallic behavior of its electric conductivity above 300 K [1]. In order to understand its physical properties, we have investigated its valence-band electronic structure by photoelectron spectroscopy.

Photoelectron measurements were carried out with use of single-crystalline specimens prepared in size of  $5 \times 0.5 \times 0.5 \text{ mm}^3$  by a flux method [1]. A Pt wire was attached to one end of the specimen to avoid the charging up at low temperatures, and the clean surface was obtained by *in situ* fracturing another end of the specimen in perpendicular to the *c* axis.

Figure 1 shows typical valence-band photoelectron spectra recorded at 20 K with the excitation photon energies  $h\nu$  of 60 and 75 eV and their difference spectrum. Each spectrum is normalized with the integrated intensity and subtracted the background by an iteration method [2]. Observed features A to C are ascribed to the hybridized bands of the Co *3d* and O *2p* states, and the Co *3p-3d* resonance photoemission shows the relatively large Co *3d* contribution to the features A and B, as seen in the difference spectrum. The other features D, E, F, G and H are assigned to the  $\text{CO}_3$ -derived states, the surface components, Ba *5p* spin-orbit doublets and O *2s* state, respectively.

Figure 2 shows temperature dependence of the valence-band spectra near the Fermi level  $E_F$  together with reference Au spectra.  $\text{Ba}_3\text{Co}_2\text{O}_6(\text{CO}_3)_{0.7}$  reveals large reduction in intensity towards  $E_F$  but clear finite intensity at  $E_F$ , which suggests the electron doping into the low-spin  $\text{Co}^{4+}(t_{2g}^5 e_g^1)$  bands and the positive thermoelectric power of 81 or  $141 \mu\text{V K}^{-1}$  at high temperatures for the  $\text{Co}^{4+}$  concentration *x* of 0.7 [3]. Although a 1/8-power-law dependence of the intensity on the binding energy  $E_B$  might be expected in one-dimensional fermion system [4], the anomalous exponents from 0.5 at 20 K to 0.8 at 200 K are obtained for  $E_B = 0.01\sim 0.1 \text{ eV}$ , which suggests the larger short-range interaction at the lower temperature. A small hump at  $E_B \sim 0.02 \text{ eV}$  observed at  $T = 20 \text{ K}$  might also indicate the opening of a

pseudogap or a magnetic ordering, which may cause the recently observed reduction in the electric conductivity at low temperatures [5].

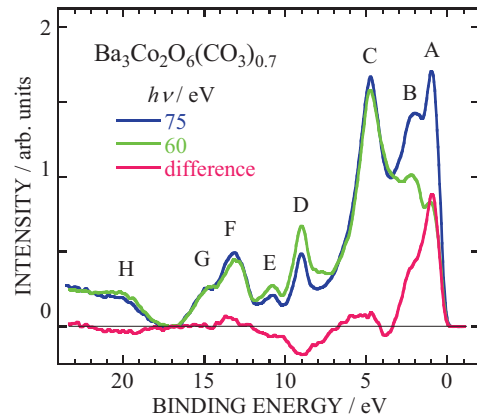


Fig.1. Valence-band spectra and difference spectrum of  $\text{Ba}_3\text{Co}_2\text{O}_6(\text{CO}_3)_{0.7}$ .

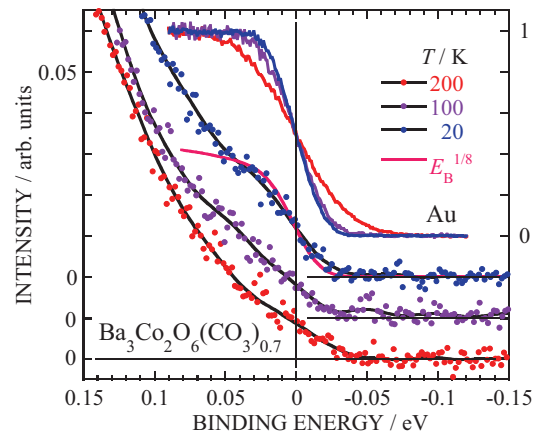


Fig.2. Temperature dependence of valence-band spectra near the Fermi level of  $\text{Ba}_3\text{Co}_2\text{O}_6(\text{CO}_3)_{0.7}$ .

[1] T. Yamamoto *et al.*, Proc. Int. Symp. on EcoTopia Science 2007, p.145.

[2] K. Soda *et al.*, J. Phys. Soc. Jpn. **60** (1991) 3059.

[3] W. Koshibae *et al.*, Phys. Rev. B **62** (2000) 6869.

[4] J. Voit, Pep. Prog. Phys. **57** (1994) 977.

[5] K. Iwasaki, *private communication*.

## Terahertz Spectroscopy of Doped Superionic Conductors

T. Awano

Department of Electronic Engineering, Tohoku Gakuin University, Tagajo 985-8537, Japan

$\text{RbA}_4\text{X}_5$  ( $\text{A}=\text{Ag}$  or  $\text{Cu}$ ,  $\text{X}=\text{halogen}$ ) crystal has high ionic conductivity as liquid even at room temperature. Silver (copper) ions move fast in conductive channels which are composed of silver (copper) sites surrounded by iodide tetrahedra. Sixteen ions in a unit cell are able to occupy 56 such sites. These available sites for the conducting ion are not enough to avoid Coulomb repulsion by each other. This suggests that collective movement of conducting ions should occur. Such correlative motion should be enhanced largely by doping excess conduction ions. In this study, terahertz spectra of excess silver (copper) doped  $\text{RbA}_4\text{X}_5$  and silver (copper) vacancy doped one were investigated to study such effect by the collective motion.

Excess silver was doped by evaporation of silver film on the crystal and diffusion by heating. Vacancy of silver was introduced by iodine vapor addition at room temperature.

Figure 1 shows reflectivity spectra of  $\text{RbAg}_4\text{I}_5:\text{Ag}$  and  $\text{RbAg}_4\text{I}_5:\text{I}_2$ . The latter corresponds to introducing silver vacancy. Figures 2 and 3 show dielectric constants obtained by Kramers-Kronig analysis. The dielectric constants decreased by silver addition and increased by iodine addition in the spectral region below  $20\text{cm}^{-1}$ . This spectral region corresponds to "attempt mode" which is a movement of a silver ion going out from surrounding iodide tetrahedral cage. Therefore spectral change of this region seems to concern dynamics of the ion conduction strongly.

In the study of Raman scattering spectra of doped  $\text{RbAg}_4\text{I}_5$ , drastic spectral changes were reported previously<sup>1, 2</sup>. The scattering intensity in terahertz region (under  $50\text{cm}^{-1}$ ) increased by silver addition and decreased by iodine addition. Moreover fine structures at low temperature disappeared in the case of iodine addition<sup>2</sup>.

The FIR results of this study are contrary to those of the Raman spectroscopic study. The intensity change of low wave number region was exactly reverse between them. The fine structure did not disappear in the FIR spectra. These differences between them seem to be due to difference of optical process between FIR and Raman spectroscopy.

[1] S. Bredikhin, T. Hattori and M. Ishigame, *Solid State Ionics* **67** (1994) 311.

[2] S. Bredikhin, N. Kovaleva, T. Hattori and M. Ishigame, *Solid State Ionics* **74** (1994) 149.

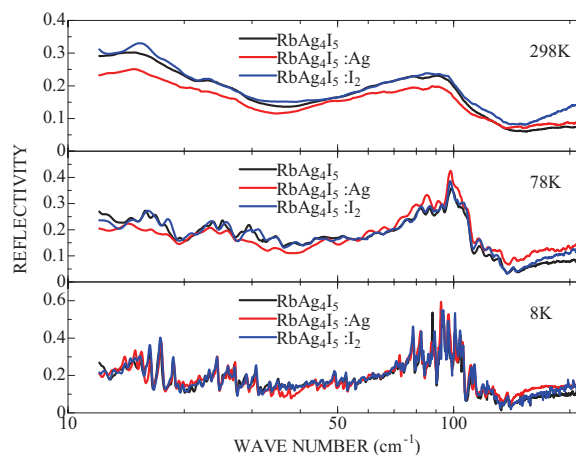


Fig. 1. Reflectivity spectra of doped- $\text{RbAg}_4\text{I}_5$ .

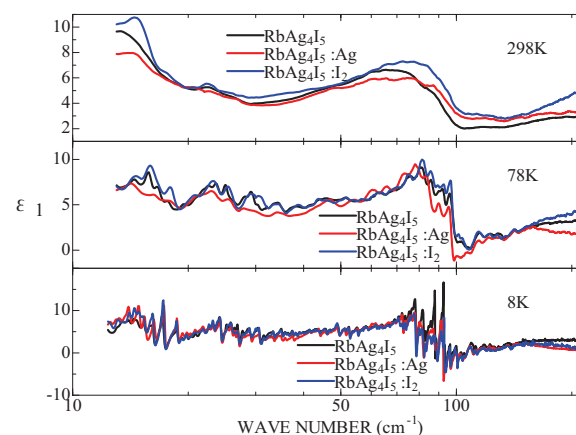


Fig. 2. Real part of dielectric constant of doped- $\text{RbAg}_4\text{I}_5$ .

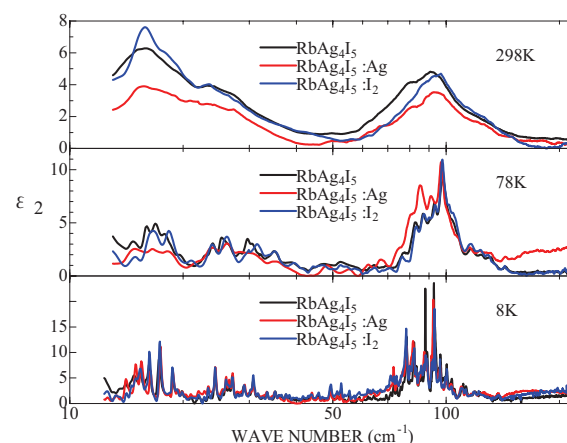


Fig. 3. Imaginary part of dielectric constant of doped- $\text{RbAg}_4\text{I}_5$ .

## Evolution of $c$ - $f$ Hybridization State of $\text{CeIn}_3$

T. Iizuka<sup>1</sup>, T. Mizuno<sup>1</sup>, C. I. Lee<sup>2</sup>, Y. S. Kwon<sup>2</sup>, S. Kimura<sup>3,1</sup>

<sup>1</sup>*School of Physical Sciences, The Graduate University for Advanced Studies (SOKENDAI), Okazaki 444-8585, Japan*

<sup>2</sup>*Department of Physics, Sungkyunkwan University, Suwon 440-746, Korea*

<sup>3</sup>*UVSOR Facility, Institute for Molecular Science, Okazaki 444-8585, Japan*

### Introduction

“Heavy fermion” attracts attention because of their various physical properties, which originate from the hybridization between the localized  $4f$  and conduction electrons, namely  $c$ - $f$  hybridization [1]. According to the periodic Anderson model (PAM), which theoretically describes the change of electronic structure with the  $c$ - $f$  hybridization, the bonding and antibonding bands due to the  $c$ - $f$  hybridization are created. The size of the energy gap increases with increasing  $c$ - $f$  hybridization intensity.

The purpose of this study is to investigate the evolution of the  $c$ - $f$  hybridization state. The hybridization intensity can be controlled by applying pressure. The target material of this study,  $\text{CeIn}_3$ , which has a localized  $4f$ -electron, is the antiferromagnetic (AFM) ground state (the Néel temperature  $T_N \sim 10$  K). With applying pressure,  $T_N$  is monotonically suppressed and is disappeared at  $P_C = 2.6$  GPa. Then a superconducting phase appears. In addition, from a NQR measurement on  $\text{CeIn}_3$  under pressure, there is  $T^*$ -line which divides the local regime ( $T^* > T$ ) and the itinerant regime ( $T^* < T$ ), at around 2 GPa in the nonmagnetic state [2]. Therefore this material is suitable to investigate the evolution of the  $c$ - $f$  hybridization state by applying pressure.

### Experimental

The single phase  $\text{CeIn}_3$  was synthesized by an arc-melting method under argon atmosphere, and then was annealed at 600 °C for three weeks inside an evacuated quartz tube. The THz reflection spectroscopy under pressure was performed at the THz micro-spectroscopy end station of BL6B, UVSOR-II. A diamond anvil cell was employed to produce high pressure. KBr was used as a pressure medium and gold as a reference. The pressure was calibrated by a ruby fluorescence method.

### Results and Discussion

We obtained pressure-dependent reflectivity spectra [ $R(\omega, P)$ ] of  $\text{CeIn}_3$  at 5.6 K in the pressure region from 0.2 to 2.7 GPa as shown in Fig. 1a. At the lowest pressure ( $P = 0.2$  GPa), the spectrum intensity monotonically decreases with increasing photon energy indicating the normal metallic character. At 0.9 GPa in the AFM phase, a peak appears at around

17meV. The peak corresponds to the optical transition between the bonding and antibonding state of the  $c$ - $f$  hybridization state. The peak shifts to higher photon energy side with increasing pressure. The peak shift is consistent with the increase of the  $c$ - $f$  hybridization intensity behavior predicted by PAM.

The  $c$ - $f$  hybridization state is evolved not only in the nonmagnetic state but also in the AFM state. This result supports the spin-fluctuation (SDW) model [1, 3], which has a phase boundary dividing the local/itinerant regime in the AFM phase.

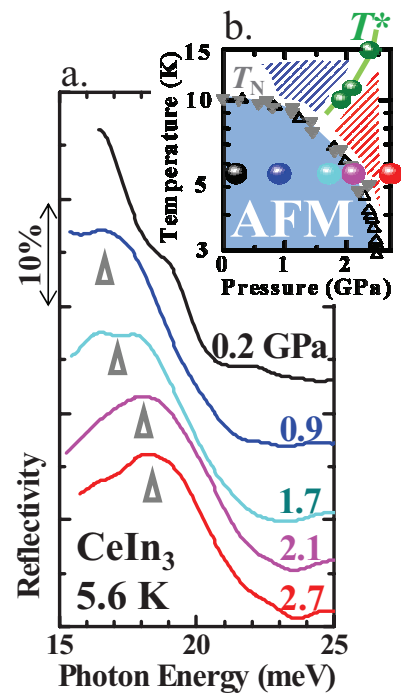


Fig. 1. (a) Pressure-dependent reflectivity spectra [ $R(\omega, P)$ ] of  $\text{CeIn}_3$  at 5.6 K. Triangles suggest peak positions. (b) Temperature-pressure phase diagram previously obtained from a NQR measurement ( $T_{\text{Néel}}$  and  $T^*$ ) [2].  $T^*$  divide local (blue mesh) and itinerant (red mesh) regime. The solid circles indicate the positions where the optical spectra were taken.

- [1] P. Gegenwart *et al.*, Nat. Phys. **4** (2008) 186.  
 [2] S. Kawasaki *et al.*, J. Phys. Soc. Jpn. **73** (2004) 1647.  
 [3] S. Watanabe and K. Miyake, J. Phys. Soc. Jpn. **79** (2010) 033707.

## Magneto-Plasma Reflection Study of Superconducting InN

T. Inushima<sup>1</sup>, T. Iizuka<sup>2</sup>, S. Kimura<sup>2,3</sup> and K. Fukui<sup>4</sup>

<sup>1</sup>Department of Electronics, Tokai University, Hiratsuka 259-1292, Japan

<sup>2</sup>School of Physical Sciences, The Graduate University for Advanced Studies (SOKENDAI), Okazaki 444-8585, Japan

<sup>3</sup>UVSOR Facility, Institute for Molecular Science, Okazaki 444-8585 Japan

<sup>4</sup>Department of Electrical and Electronics Engineering, University of Fukui, Fukui, 910-8507, Japan

Among the III-nitride semiconductors, InN is a key material for optical and high temperature device applications. Since it was reported that InN had a small band gap energy (0.64 eV) and a superconducting character [1], it has become a big issue to determine the electron effective mass. Hence we measured the electron effective mass of superconducting InN from the reflection spectra with the cyclotron resonance.

The InN film (GS1949) investigated here was grown by the Cornell University group and had a carrier density of  $\sim 4.5 \times 10^{17} \text{ cm}^{-3}$  and a mobility of  $\sim 2000 \text{ cm}^2(\text{Vs})^{-1}$ . The sample showed Meissner effect below 1.8 K. It was set in an Oxford spectromag 6T and the reflectivity was measured from 50 to 660  $\text{cm}^{-1}$  at 6 K by Jasco FTIR610 at Faraday configuration. The optical resolution was 0.5  $\text{cm}^{-1}$ .

Figure 1 shows the reflectivity spectrum at 6 K. It is analyzed using the following dielectric function ( $n_i$ ),

$$n_i^2(\omega) = \epsilon_\infty \left( 1 - \frac{\omega_p^2}{\omega(\omega \pm \omega_c + i\gamma)} + \frac{(\omega_{LO}^2 - \omega_{TO}^2)}{\omega_{TO}^2 - \omega^2 - i\Gamma\omega} \right),$$

$$\omega_c = \frac{eB}{m^*}, \quad (1)$$

where  $\omega_p$  and  $\omega_c$  are plasma and cyclotron frequencies, respectively. Reflectivity  $R$  is calculated using the following equation,

$$\frac{E_{or}}{E_{oi}} = \frac{(n_1 - n_2)(n_1 + n_0)e^{ikn_1d} + (n_2 + n_1)(n_0 - n_1)e^{-ikn_1d}}{(n_2 - n_1)(n_1 - n_0)e^{ikn_1d} + (n_2 + n_1)(n_0 + n_1)e^{-ikn_1d}},$$

$$R = \left| \frac{E_{or}}{E_{oi}} \right|^2, \quad (2)$$

where  $d$  ( $\sim 5 \mu\text{m}$ ) is the film thickness,  $n_0$  and  $n_2$  are the refractive indices of air and sapphire, respectively.

Figure 2 shows the change of the reflectivity ( $\Delta R(B) = R(B) - R(0)$ ) caused by the magnetic field. In this experiment, unpolarized light was used. Hence, when there is a plasma oscillation,  $\Delta R(B)$  has a peak near  $\omega_p$ . The two peaks ( $\sim 230 \text{ cm}^{-1}$  and  $100 \text{ cm}^{-1}$ ) in the spectrum indicate that there are two plasma oscillations in the sample investigated. Therefore we add another plasma oscillation in the dielectric function as follows,

$$n_i^2(\omega) = \epsilon_\infty \left( 1 - \frac{\omega_{p1}^2}{\omega(\omega \pm \omega_c + i\gamma_1)} - \frac{\omega_{p2}^2}{\omega(\omega \pm \omega_c + i\gamma_2)} + \frac{(\omega_{LO}^2 - \omega_{TO}^2)}{\omega_{TO}^2 - \omega^2 - i\Gamma\omega} \right), \quad \omega_c = \frac{eB}{m^*}. \quad (3)$$

Here we assume that InN has a spherical Fermi sur-

face and a unique effective mass  $m^*$ . The best fittings are obtained when  $m^* = 0.08 m_0$ ,  $\omega_{p1} = 0.016 \text{ eV}$  with  $\gamma_1 = 15 \text{ meV}$  and  $\omega_{p2} = 0.028 \text{ eV}$  with  $\gamma_2 = 3.3 \text{ meV}$ . This result indicates that the conduction band of superconducting InN has at least two electrons with different mobilities. This will explain many of the controversial problems reported for InN[2].

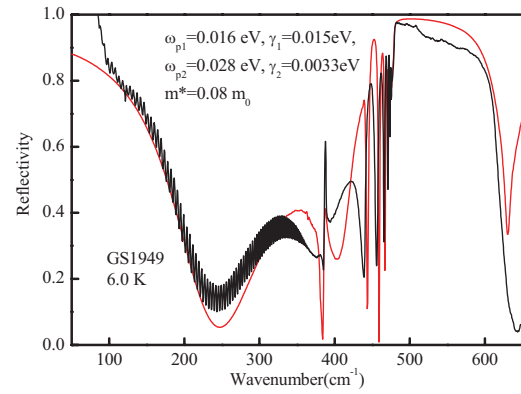


Fig. 1. Reflectivity spectrum of GS1949 at 6 K at zero magnetic field. Fitting is done using Eqs. (2) and (3) with parameters given in the figure.

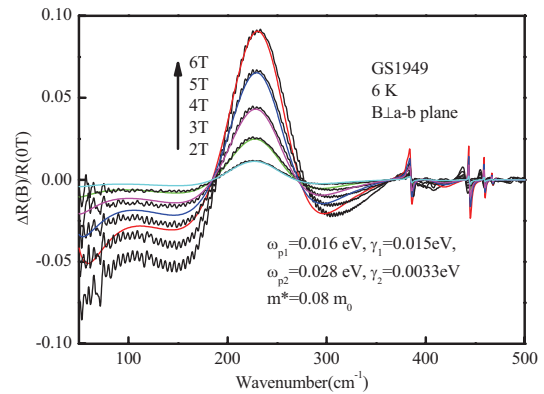


Fig. 2. Change of the reflectivity  $\Delta R(B)$  as a function of the applied magnetic field at 6K. Fittings are done using Eqs. (2) and (3) with parameters given in the figure.

[1] T. Inushima *et al.*, J. Crystal Growth **227-228** (2001) 481.

[2] C. H. Swartz *et al.*, J. Crystal Growth **269** (2004) 29.

## Optical Study of Metal-Insulator Change in $\text{LiV}_2\text{O}_4$ under High Pressure

A. Irizawa<sup>1</sup>, T. Iizuka<sup>2</sup> and S. Kimura<sup>2,3</sup>

<sup>1</sup>Graduate School of Science and Technology, Kobe University, Kobe 657-8501, Japan

<sup>2</sup>School of Physical Sciences, The Graduate University for Advanced Studies (SOKENDAI), Okazaki 444-8585, Japan

<sup>3</sup>UVSOR Facility, Institute for Molecular Science, Okazaki 444-8585, Japan

### Introduction

The optical study under multi-extreme condition such as high-pressure and low-temperature is one of the most attractive techniques for the investigation of electronic states of solids. In case of strongly correlated electron systems, the pressure will directly affect the electron-electron interactions through the change of lattice constants. Optical reflectivity experiment under high pressure can be carried out using a diamond anvil cell (DAC) because of not only the highest hardness on earth but also the high transparency in the wide energy region from terahertz (THz) to ultraviolet (UV) of the diamond. In addition the highest thermal conductivity on earth of the diamond also enables to get lower temperature in the sample space. On the other hand, there are some difficulties for this experiment. The sample space is as small as the culet of diamond which is less than several hundred  $\mu\text{m}$  in usual. At the same time, the maximum pressure is controlled by the size of culet. For example, DAC with 600  $\mu\text{m}\phi$  culet can achieve the maximum pressure up to 20 GPa, but it is risky that we go beyond 12 GPa with 800  $\mu\text{m}\phi$  one without spare. Here we should consider the diffraction limit at far-infrared (FIR) region. For example the photon energy of 10 meV is equal to the wavelength of 125  $\mu\text{m}$ . Therefore the lowest photon energy and the highest pressure are exclusive for each other. A serious problem at the scene of experiment is that the pressure and temperature are hardly controlled individually because of the hysteresis procedure of them caused by finite friction of the moving part of apparatus at low temperatures. The sample position should be also adjusted at every pressure and temperature in the case of microscopy. On the basis of these experimental restrictions, we tried the reflectivity measurement at FIR region for metal-insulator change compound  $\text{LiV}_2\text{O}_4$  under pressure at low temperature. Spinel oxide  $\text{LiV}_2\text{O}_4$  has been found for the first time to show a heavy fermion state among 3d metal oxides.  $\text{LiV}_2\text{O}_4$  has vanadium with half integer valence number of +3.5 ( $d^{1.5}$ ) in a metallic state. In an insulating state it should exhibit the alternated valence numbers of  $\text{V}^{3+}:\text{V}^{4+}=1:1$  or  $\text{V}^{3+}:\text{V}^{5+}=3:1$  together with the constant states of  $\text{Li}^{1+}$  and  $\text{O}^{2-}$ . Under pressures, the low temperature metallic phase drastically changes to an insulating one [1]. The formation of charge ordering has been predicted in this insulating phase. A structural distortion involving the distribution of V-V

bond length is confirmed by a x-ray analysis and an EXAFS experiment. We have investigated the electronic states of  $\text{LiV}_2\text{O}_4$  under pressures and low temperatures analyzed by optical study using an infrared microscope in SPring-8 [2-4]. There are three different phases showing the characteristic optical spectra. In the middle phase between the metallic and insulating ones, the spectra show a gradual change with pressure and temperature. The purpose of experiment in this beam time, we will observe this gradual change carefully inhibiting the pressure-shift as far as possible during temperature change.

### Experimental

The optical reflectivities of single crystal  $\text{LiV}_2\text{O}_4$  were measured at the microscope end station of UVSOR-II BL6B. The procedure of high pressure experiment was similar to the former studies. The observed wavenumber was between 80 and 700  $\text{cm}^{-1}$  with the fixed pressure of 8 GPa. The temperature was changed between 20 and 300 K.

### Results and Discussion

The tentative reflectivities obtained from the spectra of sample and Au film in DAC are shown in Fig. 1. Here we can confirm the gradual change from metallic spectrum at 300 K to the other ones of reduced intensities with decreasing temperature. The measurements were succeeded both in decay mode and Top-up mode.

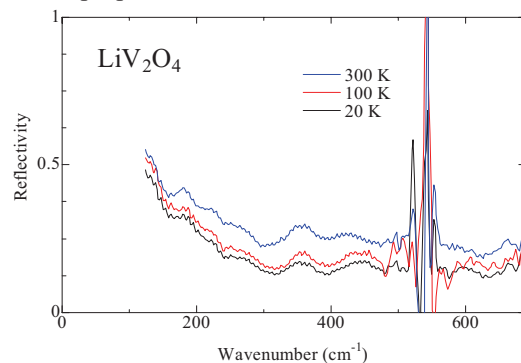


Fig. 1. Temperature change of reflectivity at FIR region under 8 GPa.

- [1] C. Urano, PhD thesis, University of Tokyo (2000).  
 [2] K. Shimai, A. Irizawa *et al.*, *Infrared Physics & Technology* **51** (2008) 468.  
 [3] A. Irizawa *et al.*, *Physica B*, **403** (2008) 948.  
 [4] A. Irizawa *et al.*, *Journal of Phys: Conf. Ser.* **150** (2009) 042070.

## Infrared Reflection Spectra of $\text{In}_x\text{Al}_{1-x}\text{N}$

K. Ozaki<sup>1</sup>, R. Ueda<sup>1</sup>, K. Fukui<sup>1</sup>, A. Yamamoto<sup>1</sup>

<sup>1</sup>*Dept. Elec. Elec. Engi, Univ. Fukui, Fukui 910-8507, Japan*

The ternary  $\text{In}_x\text{Al}_{1-x}\text{N}$  has great potential for applications in the solar cell with a wide variable bandgap range from 0.7 eV to 6.2 eV. However, many of its basic properties are still unknown, because it is difficult to obtain high quality thin films due to the huge differences of the growth conditions between InN and AlN. Our purpose in this report is to present the vibrational properties of the  $\text{In}_x\text{Al}_{1-x}\text{N}$  over a wide In fraction range using the selected thin films whose infrared reflection spectra can be explained by the fitting calculations based on the dielectric function written by both LO and TO phonon contributions [1]

$$\varepsilon(\omega) = \varepsilon_\infty \prod_j \frac{\omega_{jL}^2 - \omega^2 + i\Gamma_{jL}\omega}{\omega_{jT}^2 - \omega^2 + i\Gamma_{jT}\omega} \quad (1)$$

where  $\varepsilon_\infty$ ,  $\omega_{jL}$ ,  $\omega_{jT}$ ,  $\gamma_{jL}$ ,  $\gamma_{jT}$  are high-frequency dielectric constant,  $j$ -th branch longitudinal and transverse optical phonon (LO, TO) frequencies and  $j$ -th branch LO and TO phonon damping.

Each  $\text{In}_x\text{Al}_{1-x}\text{N}$  thin film was grown on the sapphire substrate with a GaN buffer layer by MOVPE at University of Fukui. The In fraction of the thin films were  $x = 0.90, 0.70, 0.68, 0.60, 0.35,$  and  $0.30$ . The film thickness and the carrier density are  $0.4 \sim 1.1 \mu\text{m}$  and  $10^{18} \sim 10^{19} \text{cm}^{-3}$ , respectively.

By using Eq. 1 and the transfer matrix method, the theoretical total reflectance with the consideration of the multiple reflection based on InAlN-sapphire two layers model can be described. Then, the fitting calculations between experimental and theoretical reflectance spectra have been carried out. The best fitting results suggest that the TO phonons consist of both InN-like and AlN-like TO phonons (two-mode behavior), and the LO phonon consists of one phonon (one-mode behavior). Similar one-mode LO – two-mode TO result was found in the ternary AlGaIn [2], and suggest that the TO phonon vibration is so localized and investigated theoretically [3].

The infrared reflection spectrum of  $\text{In}_x\text{Al}_{1-x}\text{N}$  ( $x = 0.6$ ) and the fitting result are shown in Figure 1. The dip at  $480 \text{ cm}^{-1}$  is attributed to the InN-like TO phonon. According to the fitting calculation, it is found that the shoulder like spectral feature at the lower wavenumber side of the  $580 \text{ cm}^{-1}$  peak is attributed to the AlN-like TO phonon, though it is not clearly seen in the spectrum. The rising edge at around  $900 \text{ cm}^{-1}$  from higher wavenumber side to lower is due to the beginning of the Reststrahlen band. Figure 2 shows the In fraction dependence of the fitted TO phonon and LO phonon wavenumber. It is clear that the In fraction dependences of both the InN-like TO phonon wavenumber and AlN-like TO

phonon wavenumber are relatively weak. On the other hand, the LO phonon wavenumber shows the clear In fraction dependence, and obvious softening above 0.7 In fraction. Such a strong softening is not predicted by Ref. 3 and further investigation is underway.

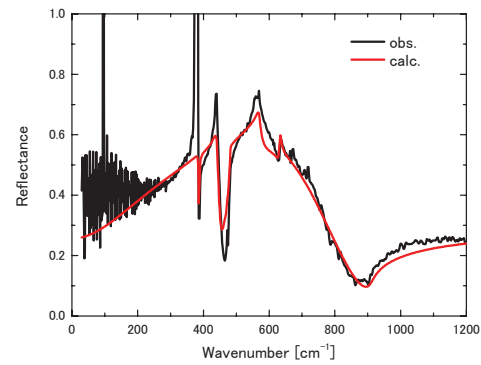


Fig. 1. Reflection spectrum of  $\text{In}_x\text{Al}_{1-x}\text{N}$  ( $x = 0.6$ ) and the fitting result.

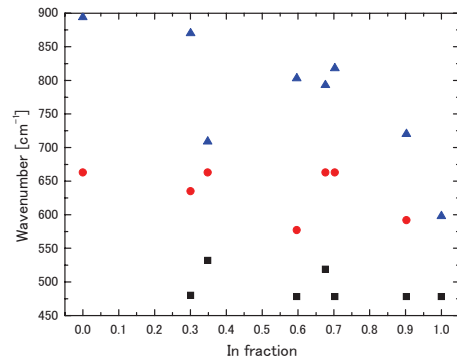


Fig. 2. Indium fraction dependence of the AlN-like TO phonon (circle), InN-like TO phonon (square), and LO phonon (triangle) wavenumber for  $\text{In}_x\text{Al}_{1-x}\text{N}$ .

[1] F. Gervais and B. Piriou, *J. Phys. C* **7** (1974) 2374.

[2] A. Cros, H. Angerer, R. Handschuh, O. Ambacher and M. Stutzmann, *Solid State Commun.* **104** (1997) 35.

[3] H. Grille, Ch. Schnittler and F. Bechstedt, *Phys. Rev. B* **61** (2000) 6091.

## Temperature Dependent Angle-Resolved Photoemission Study on $\text{BaFe}_{1.8}\text{Co}_{0.2}\text{As}_2$

T. Hajiri<sup>1</sup>, R. Niwa<sup>2</sup>, S. Murakami<sup>2</sup>, H. Miyazaki<sup>3</sup>, J. B. Hong<sup>4</sup>, Y. R. Jang<sup>4</sup>, S. Kimura<sup>3,5</sup>,  
Y. S. Kwon<sup>4</sup> and T. Ito<sup>1,6</sup>

<sup>1</sup>Graduated School of Engineering, Nagoya University, Nagoya 464-8603, Japan

<sup>2</sup>School of Engineering, Nagoya University, Nagoya 464-8603, Japan

<sup>3</sup>UVSOR Facility, Institute for Molecular Science, Okazaki 444-8585, Japan

<sup>4</sup>Department of Physics, Sungkyukwan University, Suwon 440-749, Korea

<sup>5</sup>School of Physical Sciences, the Graduate University for Advanced Studies (SOKENDAI),  
Okazaki 444-8585, Japan

<sup>6</sup>Nagoya University Synchrotron Radiation Research Center, Nagoya University, Nagoya  
464-8603, Japan

Iron pnictides superconductor discovered recently has been intensively studied both from experiment and theory, however an essential mechanism of its anomalous superconductivity has not been clarified yet. To understand the mechanism of superconductivity, the superconducting gap information, i.e., the origin of superconducting pairing is one of the most important issues. For example, multiple isotropic gaps suggesting s-wave pairing have been reported on the optimally hole-doped  $\text{Ba}_{0.6}\text{K}_{0.4}\text{Fe}_2\text{As}_2$  [1].

We have performed angle-resolved photoemission spectroscopy (ARPES) on electron-doped iron pnictides superconductor  $\text{BaFe}_{1.8}\text{Co}_{0.2}\text{As}_2$  in the slightly underdoped regime ( $T_c=25$  K), to elucidate the essential role of the doped carriers to the anomalous superconductivity [2].

Figure 1 shows the Fermi surface image of  $\text{BaFe}_{1.8}\text{Co}_{0.2}\text{As}_2$  at 35 K (normal state) obtained by plotting the intensity of ARPES spectrum at  $E_F \pm 10$  meV. Figures 2(a) and (b) show the ARPES spectra around the  $\Gamma$  and M point, respectively. From the present ARPES results, we have clearly found the hole- and the electron-pocket around the  $\Gamma$  and M point, respectively, which can be qualitatively reproduced by the band calculation on the '122' series [3]. It should be noted that the large electron-pocket expected in the calculation along cut2 disappears because of the matrix element effect with horizontal polarization of the present light source [4].

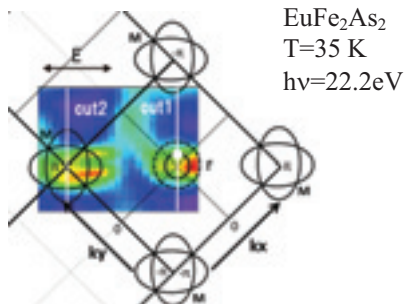


Fig. 1. Fermi surface image of  $\text{BaFe}_{1.8}\text{Co}_{0.2}\text{As}_2$  compared with the expected Fermi surface topology from the band calculation on  $\text{BaFe}_2\text{As}_2$ [3].

Figures 3(a) and (b) show the temperature dependence of ARPES spectra and their spectral DOS across  $T_c$  obtained at the hole-like FS (white circle in Fig. 1), respectively. We have observed superconducting gap opening below  $T=22.5$  K. With decreasing temperature, DOS at  $E_F$  gradually decreases and the gap size increases. We have estimated the gap size is about 5~6 meV.

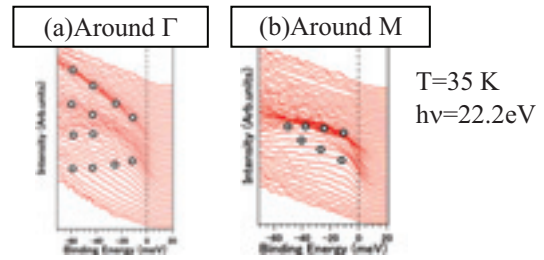


Fig. 2. ARPES spectra of  $\text{BaFe}_{1.8}\text{Co}_{0.2}\text{As}_2$  at 35 K along cut 1 (a) and cut 2 (b) in Fig. 1.

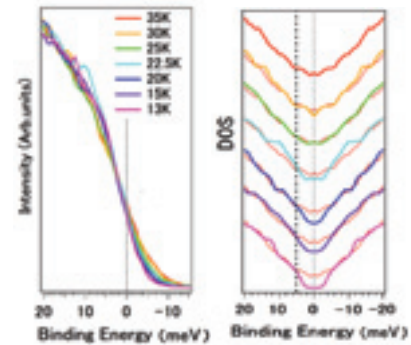


Fig. 3. (a) Temperature dependence of ARPES spectra at the hole-like Fermi surface (white circle in Fig. 1) of  $\text{BaFe}_{1.8}\text{Co}_{0.2}\text{As}_2$ . (b) Spectral DOS of Fig. 3(a) obtained by the symmetrization method [5]. Thin red lines correspond to one at 35 K.

- [1] H. Ding *et al.*, Euro Phys. Lett. **83** (2008) 47001.  
[2] Y. Kamihara *et al.*, J. Am. Chem. Soc. **130** (2008) 3296.  
[3] D. J. Singh *et al.*, Phys. Rev. B **78** (2008) 094511.  
[4] S. de Jong *et al.*, arXiv: **0912** (2009) 3434v1.  
[5] M. R. Norman *et al.*, Nature **392** (1998) 157-160.

## Angle-Resolved Photoemission Study on Possible Kondo Insulator FeSb<sub>2</sub>

S. Imada<sup>1</sup>, K. Terashima<sup>1</sup>, A. Sekiyama<sup>2</sup>, S. Suga<sup>2</sup>, A. Yamasaki<sup>3</sup>,  
K. Mima<sup>1</sup>, Y. Miyata<sup>1</sup>, R. Yamaguchi<sup>1</sup>, Y. Tachimori<sup>1</sup>, Y. Yamanoi<sup>1</sup>,  
Y. Matsui<sup>3</sup>, J. Yamaguchi<sup>2</sup>, S. Komori<sup>2</sup> and H. Nakamura<sup>4</sup>

<sup>1</sup> Faculty of Sci. and Eng., Ritsumeikan Univ., Shiga 525-8577, Japan

<sup>2</sup> Grad. School of Eng. and Sci., Osaka Univ., Osaka 560-8531, Japan

<sup>3</sup> Faculty of Sci. and Eng., Konan Univ., Kobe 658-8501, Japan

<sup>4</sup> Grad. School of Eng., Kyoto Univ., Kyoto 606-8501, Japan

Magnetic impurities in a metal trigger an upturn in the resistivity curve, so-called Kondo effect. This phenomenon has been reported in rare-earth compounds that contain localized *f*-electrons, as well as in transition metals with partial substitution of atoms. In a class of materials called Kondo insulators, Kondo effect induces an insulator-to-metal crossover under heating. Interestingly, even in some of the iron-based compounds, FeSi and FeSb<sub>2</sub>, the temperature-dependence of the resistivity resembles that of Kondo insulator. A number of experimental techniques have indicated the existence of the energy gap at the low temperature in FeSb<sub>2</sub>[1-3], while the mechanism for the formation of the energy gap remains highly controversial; whether FeSb<sub>2</sub> is a Kondo insulator[2] or a narrow-gap semiconductor[1, 3, 4]. To resolve this issue, a high-resolution angle-resolved photoemission (ARPES) study has been highly anticipated, since ARPES can directly observe the band structure and possible formation of the energy gap.

A single crystal of FeSb<sub>2</sub> has been synthesized by Sb-flux method. High-resolution photoemission study has been performed at BL7U in the UVSOR facility. Energy resolution was set at ~6 and ~15 meV for angle-integrated and angle-resolved measurement, respectively. We have obtained a clean surface of the sample by fracturing in an ultrahigh-vacuum of ~2×10<sup>-8</sup> Pa.

Figure 1 shows a typical ARPES intensity plot of FeSb<sub>2</sub> at *T* = 15 K using 17-eV photons. Several dispersive bands are clearly seen in the figure, showing that we have succeeded in the ARPES measurement of FeSb<sub>2</sub>. What is interesting is that there is a hole-like band crossing *E*<sub>F</sub> (shown by arrow in the figure) although the bulk is insulating at this temperature[1]. Such an inconsistency between PES results and bulk property is also reported in FeSi[5], where the contribution of the surface state is discussed. In fig. 1, the hole-like band lies in a *k*-region where other bands are absent. Thus we attribute the origin of metallic band to the surface.

In Fig. 2, we show a temperature-dependence of angle-integrated photoemission spectra in FeSb<sub>2</sub> taken at *hν* = 6.5 eV. As we decrease the temperature, the spectral weight near *E*<sub>F</sub> is gradually suppressed. However, a Fermi-edge cutoff remains in the spectra at *T* = 20 K, indicative of metallic state.

This metallic state may originate from the surface states shown in Fig. 1. Further study including the temperature dependence of bulk bands is necessary to clarify the origin of the energy gap in FeSb<sub>2</sub>.

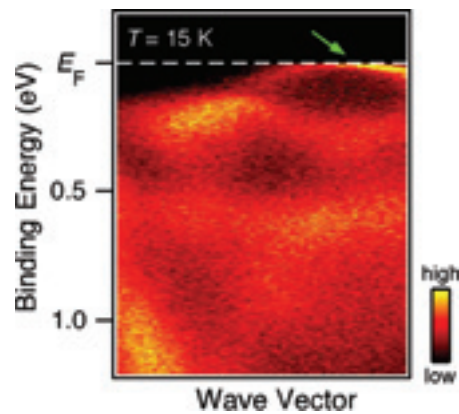


Fig. 1. ARPES intensity plot of FeSb<sub>2</sub> at *T* = 15 K (insulating phase). Green arrow points a hole-like band crossing *E*<sub>F</sub>.

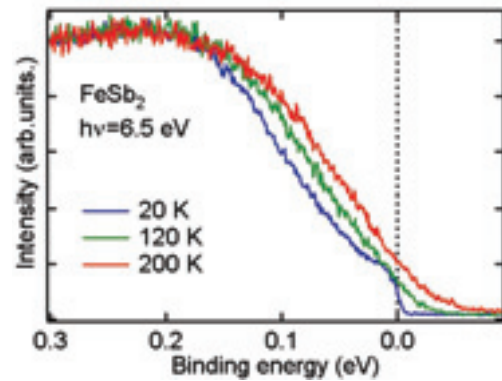


Fig. 2. Temperature-dependence of angle-integrated photoemission spectra in FeSb<sub>2</sub>.

- [1] Z. Schlesinger *et al.*, Phys. Rev. Lett. **71** (1993) 11.
- [2] C. Petrovic *et al.*, Phys. Rev. B **72** (2005) 045103.
- [3] T. Koyama *et al.*, Phys. Rev. B **76** (2007) 073203.
- [4] A. V. Lukoyanov *et al.*, Euro. Phys. J. **53** (2006) 205.
- [5] K. Ishizaka *et al.*, Phys. Rev. **72** (2005) 233202.

## High-Resolution Angle-Resolved Photoemission Study of Iron Pnictide Superconductor $\text{Ba}_{1-x}\text{K}_x\text{Fe}_2\text{As}_2$

K. Nakayama<sup>1</sup>, T. Kawahara<sup>1</sup>, T. Arakane<sup>1</sup>, T. Qian<sup>1</sup>, P. Richard<sup>2</sup>, S. Souma<sup>2</sup>, T. Sato<sup>1</sup> and T. Takahashi<sup>1,2</sup>

<sup>1</sup>*Department of Physics, Tohoku University, Sendai 980-8578, Japan*

<sup>2</sup>*WPI Research Center, Advanced Institute for Material Research, Tohoku University, Sendai 980-8577, Japan*

The discovery of superconductivity in  $\text{LaFeAsO}_{1-x}\text{F}_x$  [1] has triggered intensive researches on the high-temperature ( $T_c$ ) superconductivity of iron (Fe) pnictides. The  $T_c$  value has already exceeded 55 K by replacing La atom with other rare-earth atoms or by introducing oxygen vacancies, opening a new avenue for high- $T_c$  material research beside cuprates. Remarkable aspects of the FeAs-based superconductors are (i) electrons in the Fe orbitals, generally believed to be the foe, indeed play an essential role in superconductivity, (ii) non-doped parent compounds commonly exhibit a collinear antiferromagnetic (AF) spin density wave (SDW), and (iii) superconductivity emerges either by the hole or electron doping into the parent compounds. Angle-resolved photoemission spectroscopy (ARPES) is a key experimental technique to elucidate electronic states responsible for the occurrence of superconductivity and the AF transition. Indeed, ARPES has revealed several essential features in cuprate superconductors, like the large Fermi surface,  $d$ -wave superconducting gap, and the pseudogap above  $T_c$ .

In this study, we have performed high-resolution ARPES study of iron-based superconductor  $\text{Ba}_{1-x}\text{K}_x\text{Fe}_2\text{As}_2$  as a function of potassium concentration  $x$ . Figure 1 shows the comparison of ARPES intensity as a function of wave vector and binding energy for (a) optimally-doped superconducting  $\text{Ba}_{0.6}\text{K}_{0.4}\text{Fe}_2\text{As}_2$  ( $T_c = 37$  K) and (b) non-superconducting parent compound  $\text{BaFe}_2\text{As}_2$  ( $T_{\text{SDW}} = 138$  K) measured at  $T = 17$  K and 25 K, respectively. Corresponding energy distribution curves (EDCs) are also displayed in (c) and (d), respectively. As clearly seen in Figs. 1(a) and (b), we find a highly dispersive holelike band centered at the  $\Gamma$  point. Leading-edge midpoint of this band around the Fermi vector is clearly shifted toward higher binding energy as shown in Fig. 1(c), indicating an opening of the superconducting gap, as in previous studies [2, 3]. In contrast, in the parent compound, the band structure seems to be apparently different. We clearly find two holelike branches centered at the  $\Gamma$  point. In addition, we also observe a weaker electronlike band showing an opposite dispersion from these two holelike bands. This dramatic difference of band structure between the superconducting and the AF compounds are ascribed to the absence (appearance) of magnetic order in the

superconducting (parent) compound. The complicated band structure in the AF sample would originate in the band folding which basically follows the periodicity of new magnetic Brillouin zone. All these experimental results indicate strong influence of magnetic order / fluctuations to the fine electronic structure in the vicinity of  $E_F$  of iron-based superconductors.

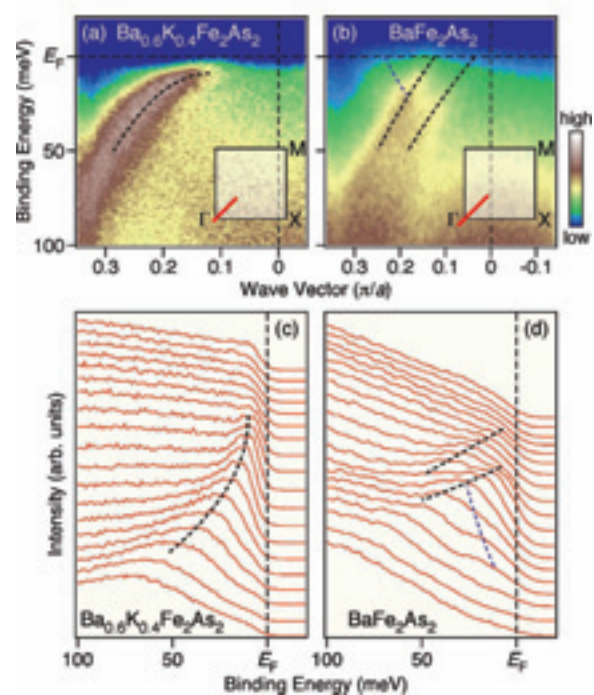


Fig. 1. ARPES intensity of (a) optimally-doped  $\text{Ba}_{0.6}\text{K}_{0.4}\text{Fe}_2\text{As}_2$  ( $T_c = 37$  K) at  $T = 17$  K and (b) parent compound  $\text{BaFe}_2\text{As}_2$  at  $T = 25$  K plotted as a function of wave vector and binding energy, measured with the 21-eV photons. Corresponding energy distribution curves are plotted in (c) and (d), respectively. Dashed lines are guides for eyes to highlight the band dispersion.

[1] Y. Kamihara *et al.*, *J. Am. Chem. Soc.* **130** (2008) 3296.

[2] H. Ding *et al.*, *Europhys. Lett.* **83** (2008) 47001.

[3] K. Nakayama *et al.*, *Europhys. Lett.* **85** (2009) 67002.

## Anisotropy of Electron Scattering and its Effect on Hall Coefficient of $(\text{Bi, Pb})_2(\text{Sr, La})_2\text{CuO}_{6+d}$ High- $T_c$ Superconductor

T. Takeuchi<sup>1,2</sup>, Y. Hamaya<sup>2</sup>, K. Ogawa<sup>2</sup>, T. Ito<sup>3</sup> and S. Kimura<sup>4</sup>

<sup>1</sup>*EcoTopia Science Institute, Nagoya University, Nagoya 464-8603, Japan*

<sup>2</sup>*Department of Crystalline Materials Science, Nagoya University, Nagoya 464-8603, Japan*

<sup>3</sup>*Department of Materials Science, Nagoya University, Nagoya 464-8603, Japan*

<sup>4</sup>*UVSOR, Institute for Molecular Science, Okazaki 444-8585, Japan*

Hall coefficient  $R_H$  of metals is generally accounted for with the well-known formula of  $R_H = 1/(ne)$ , where  $n$  and  $e$  represent carrier density and unit charge of carriers. This formula is valid only when the scattering of the electron near the Fermi level is isotropic. If we measure the Hall coefficient of the material that is characterized by the anisotropy in electron scattering, the measured Hall coefficient exceeds the value of  $R_H = 1/(ne)$ .

High- $T_c$  superconductors are typical example that possesses anisotropy of electron scattering due to the strong electron correlation. The anisotropy of electron scattering is caused by the fluctuation of the anti-ferromagnetic spin ordering, and therefore electrons near the Fermi level are scattered only in the vicinity of the anti-ferromagnetic zone boundary (AFZB). These materials indeed possess a much larger magnitude of  $R_H$  than that expected from  $R_H = 1/(ne)$ . Since the strong scattering at AFZB is getting weakened with increasing temperature or increasing carrier concentration, the Hall coefficient increases with decreasing temperature or decreasing carrier concentration.

In this study, we try to quantitatively reproduce the behaviors of Hall coefficient observed for the high- $T_c$  superconductors by using the information about both electronic structure and electron scatterings obtained by the angle resolved photoemission spectroscopy (ARPES). For this purpose, we employed the ARPES system located in BL7U of UVSOR, because it possesses an extremely good energy resolution. By using 9 eV photons as the incident beam of ARPES, we obtain the energy resolution better than a few meV.

We used the single crystal  $(\text{Bi, Pb})_2(\text{Sr, La})_2\text{CuO}_{6+d}$  superconductors, in which Pb and La are partially substituted for Bi and Sr, respectively. The former substitution effectively weakens the superstructure in Bi-O layers, which generally prevents us from easily analyzing the ARPES spectra by creating the unfavorable umklapp-bands. The latter substitution is used to decrease the hole-concentration in the sample. By employing subsequent heat-treatment, we succeed in preparing variety of samples from heavily overdoped to underdoped ones.

In this study, we selected three samples, which are one overdoped sample possessing  $T_c = 25$  K and two underdoped ones of  $T_c = 31$  K and 28 K. The ARPES

measurement was performed at at 50 K, 100 K, and 150 K with incident energy of 9 eV.

The energy distribution curves (EDC's) were successfully extracted at each Fermi wave vector. By symmetrizing the EDC spectra at the Fermi level ( $\varepsilon_F$ ), we confirmed that the consequently obtained spectra obviously possessed a peak at  $\varepsilon_F$ . The shape of the peak is well accounted for with the Lorentzian function and its FWHM is distributed over 30 ~ 50 meV. This fact indicates that the energy variation of imaginary part of self-energy, which represents the lifetime of coherent states, is roughly approximated to be constant over the narrow energy range of a few tenths of meV in width in the vicinity of  $\varepsilon_F$ .

By using the experimentally determined  $\varepsilon$ - $\mathbf{k}$  dispersion, the group velocity, and the lifetime of coherent states, we calculated  $R_H$  of the samples using the Bloch-Boltzmann equation. The resulting value is plotted in Fig.1 together with the measured ones as a function of temperature. Although the temperature dependence and hole concentration dependence of  $R_H$  were qualitatively reproduced by the calculation, the absolute value was not completely reproduced. This fact unambiguously suggests that we have to consider some other special mechanism, such as the back flow current in vertex correction.

We are now in progress for quantitatively evaluating the effect of this back flow current on  $R_H$  of present samples using the present data.

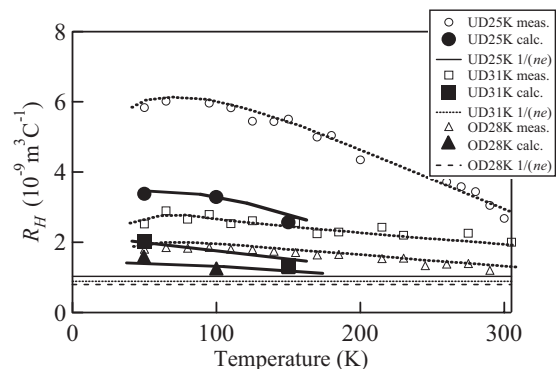


Fig. 1. The calculated and measured Hall coefficient ( $R_H$ ) of  $(\text{Bi, Pb})_2(\text{Sr, La})_2\text{CuO}_{6+d}$ . The absolute value of  $R_H$  was not reproduced by the present calculation.

## Study of VUV Reflection Spectroscopy of ZnO Thin Films Irradiated By Ar Plasma

N. Fujita, T. Yabumoto, H. Ito, T. Mizunuma, Y. Iwai,  
S. Matsumoto and H. Matsumoto

*School of Science & Technology, Meiji University, Kawasaki 214-8571, Japan*

Transparent conductive oxide (TCO) films have been widely used in the field of optoelectronic devices, such as transparent electrodes for various kinds of flat panel displays (FPDs) or photovoltaic cell [1,2].

Recently, the demands for the large-area and high-quality FPDs, transparent conductive films including tin-doped  $\text{In}_2\text{O}_3$  (ITO) films have attracted significant attention. However, due to rapid demand in recent years, the price of indium composing of ITO may raise even higher the future for a stable supply is concerned.

So, Instead of Indium as materials, ZnO is focused. ZnO is cheaper than ITO and, has the nature of the transparent conductive film by donor level is formed by oxygen vacancies or interstitial zinc in the film. As a means to lower resistance of ZnO, there is a way to include the addition of impurities and hydrogen plasma irradiation [3,4]. For Ar plasma irradiation method, no report of electrical characteristics has been made in details, and also optical properties are not reported [5].

In this study, ZnO thin films prepared by RF magnetron sputtering and fabricating by Ar plasma-irradiation. We report the optical properties of ZnO thin films for various irradiation times.

### Experiment

ZnO thin films were deposited by RF magnetron sputtering on fused quartz substrate, and at room temperature. Sintered object of zinc oxide plate were used as the target, and the sputtering was carried out in argon gas with a base pressure  $2.0 \times 10^{-2}$  Pa. The film thickness is about 390 nm.

Thin films were irradiated with Ar plasma on various times up to 20 minutes. The RF power and Ar flow rate were 20 W and 3.0 sccm. Volume resistivities were measured for ZnO thin films irradiated Ar plasma.

Reflection spectra of the films were measured in the vacuum ultraviolet region up to 25 eV with the 3-m normal incident monochromator (grating: G1 and G2) at BL-7B of UVSOR-II. A silicon photodiode sensor was used as a detector of the reflection light.

### Results and Discussion

XRD analysis showed that as deposited films were composed of polycrystalline of ZnO. Figure 1 shows the VUV reflection spectra between 5 and 25 eV of ZnO films by Ar plasma Irradiated at room temperature. The vertical axis indicates reflected

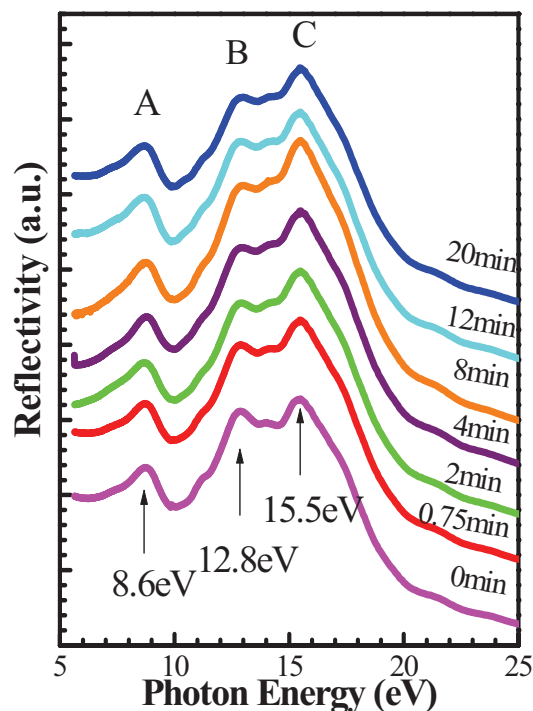


Fig. 1. VUV Reflection Spectra ZnO film by Ar plasma irradiation up to 20 min.

intensity. Three peaks A(8.6eV), B(12.8eV), C(15.5eV) appeared in all spectra. It was clearly observed that the intensity of peak increased with irradiation times of Ar plasma. Intensity of peak C is increased. However, A and B are not increased. These results are considered that the reflectivity increased with change of crystalline state with decreased irradiation times.

- [1] H. Koh, K. Sawada, M. Ohgawara, T. Kuwata, M. Akatsuka and M. Matsuhiro, SID Dig. Tech. Pap. **19** (1988) 53.
- [2] Y-M. LU *et al.*, Thin Solid Films **447- 448** (2004) 56.
- [3] P. F. Cai *et al.*, J Appl. Phys. **105** (2009) 083713.
- [4] H. Akazawa, Appl. Phys. Express **2** (2009) 081601.

## Measurement of Reflectivity of Strongly Correlated Electron Systems between Infrared and VUV Regions at BL7B

A. Irizawa<sup>1</sup> and S. Kimura<sup>2,3</sup>

<sup>1</sup>Graduate School of Science and Technology, Kobe University, Kobe 657-8501, Japan

<sup>2</sup>School of Physical Sciences, The Graduate University for Advanced Studies (SOKENDAI), Okazaki 444-8585, Japan

<sup>3</sup>UVSOR Facility, Institute for Molecular Science, Okazaki 444-8585, Japan

### Introduction

Studying optical conductivity is one of the most effective methods for understanding the electronic states of solids. In usual we measure the reflectivity between far-infrared (FIR) and near-infrared (NIR) regions using Fourier transfer type (FT) interferometer and at visible (VIS) region using the traditional grating type spectroscopy. The optical conductivity can be derived from the reflectivity through Kramers-Kronig (KK) transform where the accurate analysis can be achieved from the reflectivity in the wide energy range as far as possible. In that sense the reflectivity data from BL7B in the wide energy range between 1.2 and 40 eV (1000 nm – 30 nm) is one of the most important part for KK transform. Otherwise the reflectivity in the higher energy range should be extrapolated with a simple  $\omega^{-4}$  function. In this machine time, we prepared several solid samples of strongly correlated electron systems for both *d* electron and *f* electrons. One of them ( $\text{Ca}_{1-x}\text{Na}_x$ ) $\text{Co}_2\text{O}_4$  ( $x=0-0.5$ ) is the newly synthesized system which shows metal-insulator change with increasing Na content *x* [1].  $\text{CaCo}_2\text{O}_4$  has been known to show a temperature-dependent large thermoelectric power with semiconductor-like resistivity [2-4]. The crystal structure is Ca-ferrite-type which belongs to one of the high pressure phases of spinel structure. It includes  $\text{Co}_2\text{O}_4$  double chain component along *b* axis which consists  $t_{2g}$  orbital connection of Co 3*d* electrons. In that sense the success of carrier doping to this compound is interested in view of 1D conductor. Similar orbital network is also seen for the  $\text{Na}_x\text{CoO}_2$  which has a 2-dimensional  $t_{2g}$  orbital connection. For substituting  $\text{Ca}^{2+}$  to  $\text{Na}^+$ , doping of hole carriers can be expected into  $\text{Co}^{3+}$   $t_{2g}$  low spin state. Actually the resistivity decreases drastically with increasing *x* and the insulating behavior transforms to a metallic one at  $x=0.5$ . The other samples are selected from the also newly synthesized compounds.  $\text{CeT}_2\text{Al}_{10}$  (*T*=Fe,Ru, Os) is the series having cage-structure of *T*-Al in which Ce 4*f* electron acts an important role of electronic properties such as Kondo insulator and heavy fermion behavior [5]. In the beam time, we measured the reflectivities of all these compounds using 3-m normal incidence monochromator at BL7B.

### Experimental

The optical reflectivities of ( $\text{Ca}_{1-x}\text{Na}_x$ ) $\text{Co}_2\text{O}_4$  and  $\text{CeT}_2\text{Al}_{10}$  were measured at UVSOR-II BL7B. The energy was changed from 1.2 to 40 eV with three gratings (1200, 600, and 300 lines/mm). There are several type of optical windows for avoiding the higher degree diffractions. In the former studies, the obtained spectra using 4 type optical windows with 3 gratings were hardly connected without complex process. This time we select 3 type windows with 2 gratings for simplifying.

### Results and Discussion

As a result, the spectra can be connected without any compensation of raw data even in the case of small polycrystal samples. Figure 1 is one of the obtained results. The wide energy scan using G3 seems to be good agreement with the other results with 3 different pairs of optical windows and gratings. We are using these results of both series of compounds for getting optical conductivities with the experiments in the lower energy reflectivity measurements.

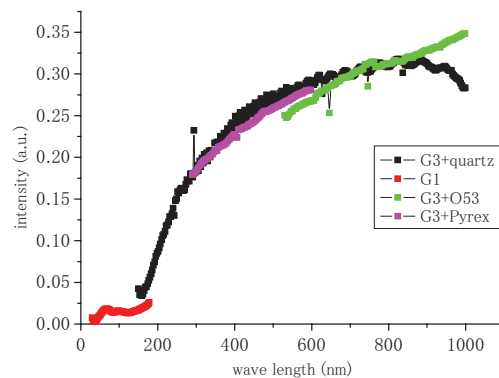


Fig. 1. Comparison of reflectivities with different optical windows and gratings.

- [1] M. Isobe *et al.*, the oral presentation in the conference of physical society of Japan (2009) 26aRG-5.
- [2] M. Shizuya, M. Isobe *et al.*, J. Solid State Chem., **180** (2007) 2550.
- [3] M. Isobe *et al.*, Physica C, **469** (2009) 948.
- [4] M. Isobe *et al.*, J. ELECTRONIC MATERIALS, **38** (2009) 1166.
- [5] Y. Muro *et al.*, JPSJ **78** (2009) 083707; ICM 09 proceedings.

# Photoluminescence and Photoluminescence Excitation Spectra of AlN

T. Ito, R. Ikematsu, S. Sawai and K. Fukui

*Dept. Elec. Elec. Engi., Univ. Fukui, Fukui 910-8507, Japan*

Aluminum nitride (AlN) has the widest direct band-gap in III-V nitride compound semiconductors. Therefore, the AlN is expected to utilize for deep UV light emitting diodes (LED) *etc.* It is known that the uppermost valence band (VB) of AlN splits into three bands (CH, HH and LH bands from bottom to top of the uppermost VB), and the transition between each level and the conduction band (CB) has the different polarization character, and knowledge of these transitions is important for fabricating the opt-electronic devices. These three transitions are usually labeled as A (from CH to CB), B (HH to CB), and C transition (LH to CB). Our purpose in this work is to present the uppermost VB structure of wurtzite AlN including A to C transition energies and their polarization characters. For this purpose, not only optical reflectance (OR) measurements but also photoluminescence (PL) and PL excitation (PLE) measurements are performed.

The AlN films were grown on the Al<sub>2</sub>O<sub>3</sub> substrates by the MOVPE. The *c*-axis of the AlN is perpendicular to the sample surface, and the thickness is about 1 μm. Highly linear polarized incident light of BL7B were used to excite the samples with  $\theta = 8^\circ$  and  $60^\circ$  in respect to the sample surface in the *p* configuration, where  $\theta$  is an incident angle.

Figure 1 shows the PL spectra at  $\theta = 8^\circ$  and  $60^\circ$ . The measurement temperature is 20K. There is no incidence angle dependence between two PL spectra. The emission bands at 5.94 eV and 5.84 eV are first and second LO phonon replicas, and the main emission band is at 6.05 eV. The inset of Fig. 1 shows the ratio between the 1-LO phonon replica band and the main band as a function of the photon energy.

Figure 2 shows that the PLE spectra at  $\theta = 8^\circ$  and  $60^\circ$ . The PLE spectra are mainly monitored at the peak photon energy of main band (6.05 eV). However, the PLE spectra at the lower photon energy side are monitored at the peak photon energy of 1-LO band (5.94 eV). The measurement temperature is 20K. Since the *c*-axis of the sample is perpendicular to the sample surface, the PLE Intensity at  $\theta = 8^\circ$  mostly consists of the  $E \perp c$  component ( $I_{E \perp c}$ ), where  $E$  is the electric field of the incident light. On the other hand, since that at  $\theta = 60^\circ$  consists of both the  $E \perp c$  and the  $E // c$  components ( $I_{E // c}$ ), the comparison between the spectra at  $\theta = 8^\circ$  and  $60^\circ$  shows the contribution of the components. Therefore, using an expression,

$$I(\theta) = I_{E \perp c} \cos^2 \theta + I_{E // c} \sin^2 \theta,$$

we also show calculated  $I_{E // c}$  in Fig. 2. The inset of Fig. 2 shows the normalized  $I_{E \perp c}$  and  $I_{E // c}$  for convenience. It is clear that only the  $I_{E // c}$  component

is excited at the lower excitation photon energy. Comparison between these PLE spectra and the OR spectra, the peaks at 6.24 eV and 6.28 eV of the  $I_{E \perp c}$  spectra in Fig. 2 are attributed to the B and C transition, respectively, and a 6.07 eV peak of the  $I_{E // c}$  spectrum is to the A transition. These assignments are in good agreement with other work [1]. However, other peaks at 6.20 eV and 6.40 eV are also observed. The 6.20 eV transition is allowed under the  $E // c$  condition, and the 6.40 eV transition is under both the  $E // c$  and the  $E \perp c$  conditions. It seems that the polarization characters of these two unknown transitions correspond to A and B (or C) transitions, respectively.

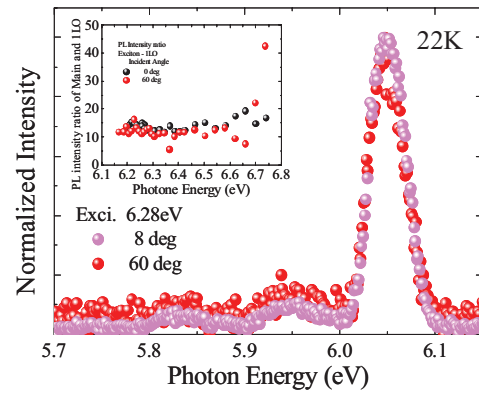


Fig 1. Incident angle dependence of PL spectra, and the PL intensity ratio of main and 1-LO bands as a function of the photon energy (inset).

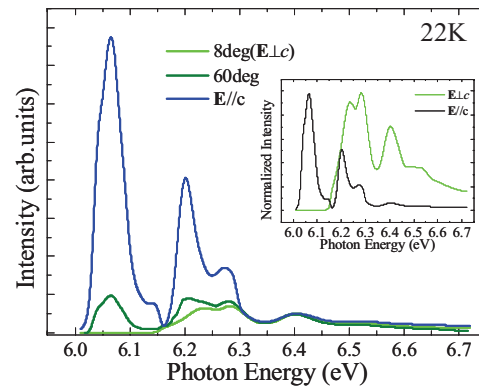


Fig 2. Incident angle dependence of PLE spectra, and normalized  $E // c$  and  $E \perp c$  components of PLE spectra (inset).

- [1] T. Onuma, T. Shibata, K. Kosaka, K. Asai, S. Sumiya, M. Tanaka, T. Sota, A. Uedono and S. F. Chichibu, *J. Appl. Phys.* **105** (2009) 023529.

## Pressure Tuning of an Ionic Insulator into a Heavy Electron Metal: An Infrared Study of YbS

H. Okamura<sup>1</sup>, M. Matsunami<sup>2</sup>, A. Ochiai<sup>3</sup> and T. Nanba<sup>1</sup>

<sup>1</sup>Graduate School of Science, Kobe University, Kobe 657-8501, Japan

<sup>2</sup>Institute of Solid State Physics, The University of Tokyo, Kashiwa 277-8581, Japan

<sup>3</sup>Center for Low Temperature Science, Tohoku University, Sendai 980-8578, Japan

YbS at ambient pressure is an ionic insulator ( $\text{Yb}^{2+}\text{S}^{2-}$ ) with the NaCl crystal structure, and has a band gap of about 1.4 eV [1, 2]. A previous optical study [1] showed that the band gap of YbS decreased under increasing external pressure. The extrapolation of the shifts of the fundamental absorption edge with pressure suggested a gap closing at  $\sim 10$  GPa. In addition, volume compression data and X-ray absorption data suggested that the Yb mean valence in YbS increased from 2 above 10 GPa, and reached  $\sim 2.4$  at 20 GPa [2]. Namely, YbS above 10 GPa was in an intermediate-valence (IV) state, where the valence of each Yb ion is fluctuating between 2 and 3. However, since the previous optical study was performed at photon energies above 0.5 eV only, it was unclear whether or not the gap actually closed at  $\sim 10$  GPa, and whether or not the IV state above 10 GPa was metallic. To answer these questions and to clarify the low-energy electronic structures of YbS under high pressure, we have carried out IR reflectivity studies of YbS [3]. The reflectivity spectra  $R(\omega)$  under high pressure were measured at the IR beam line of SPring-8, while those at ambient pressure were measured using the apparatus at Kobe University below 2 eV, and using BL7B above 2 eV up to 30 eV. High pressure was generated with a diamond anvil cell (DAC). Optical conductivity spectra  $\sigma(\omega)$  were derived from the measured  $R(\omega)$  using Drude-Lorentz fitting technique.

Figure 1 shows the measured  $\sigma(\omega)$  under pressure, together with that measured in the vacuum. The narrow peak below 0.1 eV, which are seen above 8 GPa, is a Drude peak due to free carriers. This result explicitly demonstrates that the high pressure phase in YbS has a metallic ground state. The energy gap is closed at 8 GPa, rather than at 10 GPa as previously conjectured [2]. In addition, two pronounced absorption peaks are seen to grow with pressure above 10 GPa. Namely, the high pressure phase above 10 GPa is not a simple metal, but it has some peculiar features in the electronic structures near the Fermi edge. The detailed analyses of the data show that the carriers giving rise to the Drude peak has a large effective mass of the order of  $10 m_0$ , where  $m_0$  is the rest electron mass. [3] It can be shown that the observation of the Drude peak due to such heavy electrons, and that of the pronounced absorption peaks, can be understood together using a

model based on the hybridization of the  $f$  state with a conduction band, which is also consistent with the IV previously observed above 10 GPa.

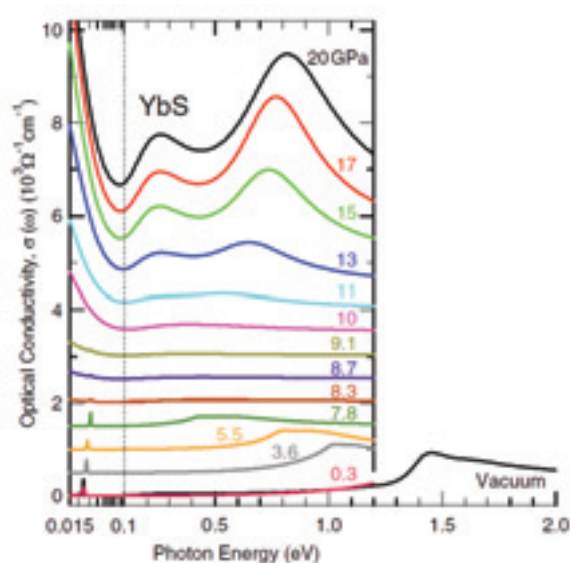


Fig. 1. Optical conductivity spectra  $\sigma(\omega)$  of YbS at room temperature at different pressures, obtained with Drude-Lorentz fitting to the measured reflectivity spectra. The spectra are offset for clarity. Note the logarithmic scale below 0.1 eV.

[1] K. Syassen, H. Winsen, H. G. Zimmer, H. Tups, and J. M. Leger, *Phys. Rev. B* **32** (1985) 8246.

[2] K. Syassen, *Physica B+C* **139-140** (1985) 277.

[3] M. Matsunami, H. Okamura, A. Ochiai and T. Nanba, *Phys. Rev. Lett.* **103** (2009) 237202.

## Angular Dependence of Spectral Responsivity and Reflectance for UV Photodetectors

T. Saito<sup>1</sup>, K. Ozaki<sup>2</sup>, S. Sawai<sup>2</sup>, K. Fukui<sup>2</sup> and I. Saito<sup>1</sup>

<sup>1</sup>National Metrology Institute of Japan, National Institute of Advanced Industrial Science and Technology, Tsukuba 305-8563, Japan,

<sup>2</sup>Faculty of Engineering, Univ. of Fukui, Fukui 910-8507, Japan

### Introduction

Needs for quantitative measurements in the UV-VUV region are increasing in various fields like UV curing, disinfection, surface cleaning etc.. In these applications, UV irradiance meters are often used quite near the source, which means that the irradiance meters receive wide divergent beams. It is, therefore, very important to check if the meters satisfy the so-called cosine law, which is required as an ideal photodetector. In addition, internal quantum efficiency,  $\eta_{\text{int}}$ , that is a fundamental measure to evaluate detector performance, can be obtained by the two measurement results of the external quantum efficiency,  $\eta_{\text{ext}}$ , and the reflectance,  $R$ , from the equation,

$$\eta_{\text{int}} = \frac{\eta_{\text{ext}}}{1 - R}$$

### Experimental

We have characterized various kinds of UV detectors (photoconductive diamond detectors, AlN, AlGaIn & GaAsP Schottky photodiodes, Si photodiodes), especially about their dependence on angle of incidence of spectral responsivity and of spectral reflectance by using p-polarization dominant radiation from the McPherson type monochromator beamline at BL7B.

### Results and Summary

Figure 1 shows measurement results of spectral reflectance for a photoconductive HOD (Highly Oriented Diamond) detector at the angles of incident of 15, 30, 45 and 60 degrees. Also shown by a dashed line is a calculated spectrum at normal incidence. More detailed calculation results including s-polarization components are shown in Fig. 2. It has been confirmed that relative spectra agree well between the measurements and the calculations. Lower reflectance for the measurements can be attributed by its diffusive surface, which is easily visible.

The results also show that reflectance loss for p-polarization decreases as the angle of incidence increases at most of the wavelengths and hence it results in increase in detector responsivity, which was also experimentally confirmed.

In conclusion, angular measurements for reflectance and responsivity are powerful technique to characterize not only internal quantum efficiency

but also important polarization property and other optical property like a overlayer thickness and its absorption.

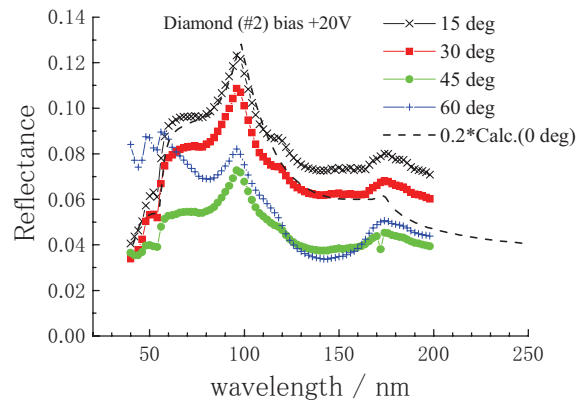


Fig. 1. Measured spectral reflectance spectra for a diamond detector (Calculated spectrum at normal incidence is also shown in dashed line).

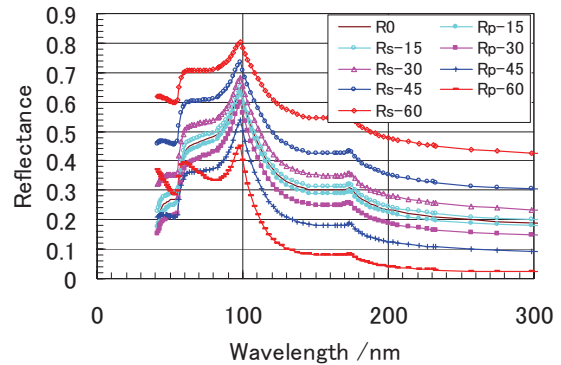


Fig. 2. Calculated spectral reflectance spectra for a diamond detector for both p- and s-components.

### Acknowledgement

Authors are grateful to Dr. Kazushi Hayashi at Kobe Steel Ltd. for providing the diamond photodetectors.

- [1] T. Saito and K. Hayashi, Appl. Phys. Lett. **86** (2005) 122113.
- [2] T. Saito *et al.*, Diamond & Related Materials **14** (2005) 1984.
- [3] T. Saito *et al.*, Metrologia **43** (2006) S51.
- [4] T. Saito *et al.*, Phys Status Solidi C **6** (2009) S658.
- [5] T. Saito *et al.*, Metrologia **46** (2009) S272.

## Photoluminescence and Photoluminescence Excitation Spectra from AlN Doped with Gd<sup>3+</sup>

S. Sawai<sup>1</sup>, T. Ito<sup>1</sup>, K. Fukui<sup>1</sup>, S. Emura<sup>2</sup>, T. Araki<sup>3</sup> and A. Suzuki<sup>4</sup>

<sup>1</sup>Dept. Elec. Elec. Engi., Univ. Fukui, Fukui 910-8507, Japan

<sup>2</sup>Inst. Sci. Indust. Res., Osaka Univ., Osaka 567-0047, Japan

<sup>3</sup>Dept. Photonics, Ritsumeikan Univ., Shiga 525-8577, Japan

<sup>4</sup>Res. Organi. Sci. Engi., Ritsumeikan Univ., Shiga 525-8577, Japan

III-V nitride compound semiconductor doped with rare elements are attractive systems because of the possibility of magnetic ordering coupled with a semiconducting nature and luminescence properties. In the ultraviolet region, a wide bandgap matrix semiconductor in combination with a Gd element is one of the target systems. In the case of Al<sub>1-x</sub>Gd<sub>x</sub>N there are several cathodeluminescence (CL) [1-4], electroluminescence [5], and photoluminescence (PL) [6] properties, in this case every result shows a sharp line at 3.90~3.94eV which is clearly observed and well assigned to the <sup>6</sup>P<sub>7/2</sub>→<sup>8</sup>S<sub>7/2</sub> 4*f* intra transition of Gd<sup>3+</sup>. However, the electronic structure of Al<sub>1-x</sub>Gd<sub>x</sub>N is still not clear. In consequence, we have performed not only PL measurements but also PL excitation (PLE) measurements of Al<sub>0.98</sub>Gd<sub>0.02</sub>N and Al<sub>0.87</sub>Gd<sub>0.13</sub>N.

Al<sub>1-x</sub>Gd<sub>x</sub>N thin films were grown in a MBE system with a RF-plasma assisted radical cell on the Si-face of (0001)-oriented 6H-SiC substrates. The thicknesses of the samples are about 120 nm.

Figure 1 shows the PL spectra of (a) Al<sub>0.98</sub>Gd<sub>0.02</sub>N and (b) Al<sub>0.87</sub>Gd<sub>0.13</sub>N at 8K. The excitation photon energy is 6.27eV. The PL spectra mainly consist of two parts. The first part is the sharp lines seen at around 3.95 eV. These sharp lines are in agreement with previous research [1] and other results [2-6], as mentioned above. The second part is the broad emission bands observed in the lower energy side which may have been weakly observed in previous CL work [1]. Since the band width of the broad emission band in (b) is much wider than in (a), it is supposed that this band is correlated to the Gd concentration. The PLE spectra and the OR spectra from Al<sub>0.98</sub>Gd<sub>0.02</sub>N at 23 K are shown in Figs. 2(a) ( $\theta = 8^\circ$ ) and 2(b) ( $\theta = 60^\circ$ ). The emission photon energies are 3.95 eV and 2.76 eV which correspond to the peak energy positions of the sharp line and the broad band, respectively. Notable features in Fig. 2 are as follows: (i) PLE spectra monitored at 2.76 eV clearly show the band edge. (ii) PLE spectra monitored at 3.95 eV also show the band edge with a peak structure at 6.3 eV. (iii) Additional peaks and shoulders at 6.11 eV are obviously found in the PLE spectra at  $\theta = 60^\circ$ . These (i) ~ (iii) features suggest that the crystal structure of Al<sub>0.98</sub>Gd<sub>0.02</sub>N is basically

similar to that of AlN, and the uniaxial anisotropy character of AlN is still present.

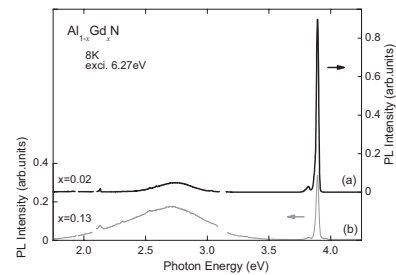


Fig. 1. Photoluminescence spectra from (a) Al<sub>0.98</sub>Gd<sub>0.02</sub>N and (b) Al<sub>0.87</sub>Gd<sub>0.13</sub>N at 8K.

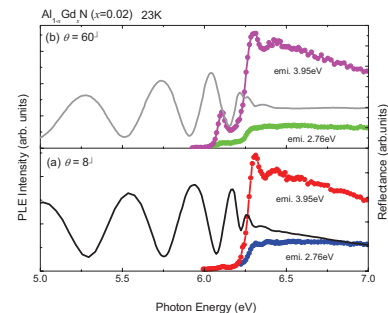


Fig. 2. Photoluminescence excitation spectra and optical reflectance spectra from Al<sub>0.98</sub>Gd<sub>0.02</sub>N at 23 K. The angles of incidence  $\theta$  are (a)  $8^\circ$  and (b)  $60^\circ$ .

[1] S. W. Choi, S. Emura, S. Kimura, M. S. Kim, Y. K. Zhou, N. Teraguchi, A. Suzuki, A. Yanase and H. Asahi, *J Alloys Compounds* **408-412** (2006) 717.

[2] U. Vetter, J. Zenneck and H. Hofsäss, *Appl. Phys. Lett.* **83** (2003) 2145.

[3] J. B. Gruber, U. Vetter, H. Hofsäss, *Phys. Rev. B* **69** (2004) 195202.

[4] T. Kita, S. Kitayama, M. Kawamura, O. Wada, Y. Chigi, Y. Kasai, T. Nishimoto, H. Tanaka and M. Kobayashi, *Appl. Phys. Lett.* **93** (2008) 211901.

[5] T. Toyama, J. Ota, D. Adachi, Y. Niioka, D. H. Lee and H. Okamoto, *J. Appl. Phys.* **105** (2009) 084512.

[6] J. M. Zavada, N. Nepal, J. Y. Lin, H. X. Jiang, E. Brown, U. Hömmerich, J. Hite, G. T. Thaler, C. R. Abemathy, S. J. Pearton and R. Gwilliam, *Appl. Phys. Lett.* **89** (2006) 152107.

## Electronic Structure of Yttrium and Carbon Atoms Encapsulated Metallofullerenes, $Y_2C_2@C_{82}$ : Ultraviolet Photoelectron Spectroscopy and Theoretical Calculation

S. Hino<sup>1</sup>, T. Miyazaki<sup>1</sup>, Y. Aoki<sup>1</sup>, N. Wanita<sup>2</sup>, M. Kato<sup>2</sup>, R. Sumii<sup>3</sup>, T. Akachi<sup>4</sup>, T. Inoue<sup>4</sup>,  
Y. Ito<sup>4</sup>, T. Sugai<sup>4</sup> and H. Shinohara<sup>4</sup>

<sup>1</sup> Graduate School of Science & Technology, Ehime University, Matsuyama 790-8577 Japan

<sup>2</sup> Graduate School of Science & Technology, Chiba University, Chiba 263-8522 Japan

<sup>3</sup> Photon Factory, Institute for Materials Structure Science, Tsukuba 305-0801 Japan

<sup>4</sup> Graduate School of Science, Nagoya University, Nagoya 464-8602 Japan

Extensive UPS study of metallofullerenes established an empirical rule that the cage structure is principally responsible for the electronic structure of mono-metal atom encapsulated metallofullerenes. That is, metallofullerenes of the same cage symmetry with an incorporated metal atom of the same oxidation state give essentially the same UPS. This empirical rule also holds in  $Y_2C_2@C_{82}$  (III) and  $Y_2@C_{82}$  (III), both of which have the same  $C_{2v}$  cage structure. However, it does not hold in  $Ti_2C_2@C_{78}$  and  $La_2@C_{78}$  although these endohedral fullerenes have the same  $D_{3h}$  (78:5) structure [11]. The case of  $Ti_2C_2@C_{78}$  and  $La_2@C_{78}$  is considered rather exceptional, since Ti atoms are fond of forming carbide and hybridization of orbitals derived from entrapped Ti and caged C atoms deforms the electronic structure of the fullerene cage so much. It is worthwhile to examine whether the empirical rule holds in three  $Y_2C_2@C_{82}$  isomers.

Figures 1 and 2 show the valence band UPS of  $Y_2C_2@C_{82}$  (I) and  $Y_2C_2@C_{82}$  (II) obtained with  $h\nu = 20 - 55$  eV photon energy. Their spectral onsets were 0.88 eV and 0.67 eV, respectively, and the previously reported value of  $Y_2C_2@C_{82}$  (III) was 0.8eV [7]. The absorption spectral edge of these three isomers is 1400 nm (0.89 eV), longer than 2000 nm (0.62 eV) and 1100 nm (1.13 eV), respectively.

The UPS of  $Y_2C_2@C_{82}$  (I) and  $Y_2C_2@C_{82}$  (II) in 0 – 15 eV energy region show 10 explicit structures labeled by A – J in the figure. Their positions deviate slightly and their intensity changes when the incident photon energy is tuned, as has been observed in the UPS of other fullerenes [7-11, 15].

Theoretical calculation on  $Y_2C_2@C_{82}$  (II) assuming  $D_{3h}$  cage structure reproduced the UPS very well. Optimized structure of entrapped  $Y_2C_2$  was found to be distorted tetragonal form.

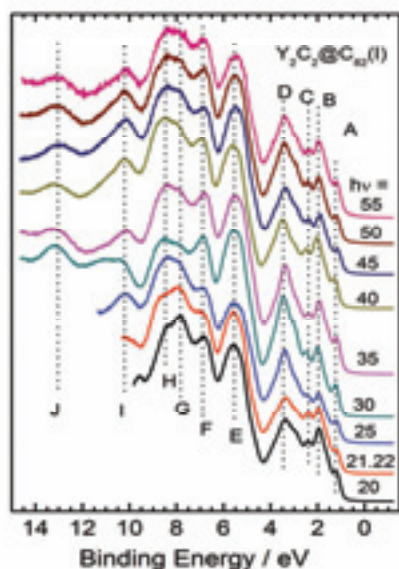


Fig. 1. UPS of  $Y_2C_2@C_{82}$  (I)

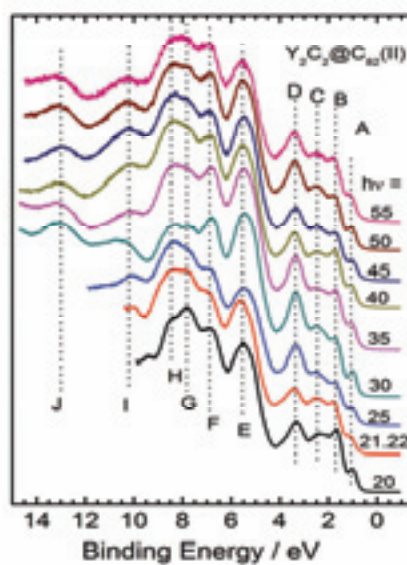


Fig. 2. UPS of  $Y_2C_2@C_{82}$  (II)

[1] S. Hino *et al.*, Phys. Rev. B **75** (2005) 125418.